

Light-cone sum rules with B -meson distribution amplitudes for the $B \rightarrow p$ form factors in B -mesogenesis models

Aritra Biswas, Alexander Khodjamirian and Ali Mohamed

*Center for Particle Physics Siegen (CPPS), Theoretische Physik 1,
Universität Siegen, D-57068 Siegen, Germany*

New decay modes of B -meson into a baryon and invisible dark antibaryon Ψ are among the most distinctive signatures of the B -mesogenesis scenario. We concentrate on the proton mode and consider two versions of the underlying interaction of Ψ with quarks, the so-called models (d) and (b). To estimate the width of the $B^+ \rightarrow p\Psi$ decay, we obtain the $B^+ \rightarrow p$ transition form factors, applying QCD light-cone sum rules (LCSRs) with B -meson distribution amplitudes with an accuracy up to twist-5, while interpolating the proton with a current. This method is independent of the previously applied one, which was based on the nucleon distribution amplitudes. We estimate the partial width of the $B^+ \rightarrow p\Psi$ decay as a function of the dark antibaryon mass. Furthermore, we use the ratio of this width to the inclusive $B \rightarrow X_N\Psi$ width, the latter predicted earlier using the heavy quark expansion method. This ratio, which is independent of the effective coupling, when combined with the minimal inclusive branching fraction of $O(10^{-4})$, necessary for the feasibility of B -mesogenesis, yields lower limits on the $B^+ \rightarrow p\Psi$ branching fraction. We confront these limits with the most recent upper bounds obtained from BaBar and Belle/Belle II searches for the decays of B^+ -meson into a proton and missing energy. The comparison indicates that experimental upper bounds on the branching fraction of $B \rightarrow p\Psi$ at the level of $10^{-8} - 10^{-7}$ are needed for a decisive probe of this invisible mode of B decays.

1. Introduction

The B -mesogenesis scenario suggested in [1, 2] (see also [3, 4]) has caused a lot of interest, offering a possibility to simultaneously solve two fundamental problems: the baryon asymmetry and the dark matter abundance in the Universe. Moreover, the B -meson decay modes into a light baryon and dark antibaryon Ψ predicted in this scenario are accessible in current experimental searches for invisible B decays. The most recent search [5] for these decays by Belle II collaboration (using the data of Belle experiment) yields upper limits reaching $O(10^{-6})$. Earlier measurements with less restrictive results included searches for $B^+ \rightarrow p\Psi$, $B^0 \rightarrow \Lambda\Psi$ and $B^+ \rightarrow \Lambda_c^+\Psi$ at the BaBar experiment (see [6], [7], and [8], respectively) and the search for $B^0 \rightarrow \Psi\Lambda$ at Belle [9].

On the theory side, the main task is to estimate the branching fraction of a B decay into a light baryon and Ψ for a given effective interaction of quarks with Ψ . In this paper, we focus on the decay mode $B^+ \rightarrow p\Psi$, which has the largest available phase space and therefore allows for the largest accessible values of the Ψ mass. We consider the two versions of a possible Ψ -triquark interaction proposed in [1, 2]. The same versions were considered in [10], where they were denoted as the B -mesogenesis models (d) and (b). In the first (second) model, the d -quark (b -quark) is directly coupled to Ψ and a heavy mediator. The effective pointlike Ψ -triquark interaction that leads to the $B^+ \rightarrow p\Psi$ decay is then formed by the coupling of the $d\Psi$ ($b\Psi$) pair via heavy mediator to the ub (ud) diquark.

Given the effective operators of the Ψ -triquark interaction, one still needs reliable estimates of the $B \rightarrow$ baryon transitions form factors. To this end, the QCD-based method of light-cone sum rules (LCSRs) was used in [10] (see also [11, 12]). The sum rules for $B \rightarrow p$ form factors were obtained, applying a vacuum-to-proton correlation function, where the effective operator of the new interaction was combined with the B -meson interpolating current. In the resulting LCSRs, nonperturbative input included the light-cone distribution amplitudes (DAs) of the proton, i.e. of the nucleon in the adopted isospin symmetry limit. In the latest analysis of these LCSRs [12], the accuracy of the operator product expansion (OPE) was upgraded from the initial twist-3 level to include all terms up to twist-6. As a result, large higher-twist contributions were revealed, signaling a slow convergence of twist expansion. Note also that the nucleon DAs used in the LCSRs depend on multiple parameters, determining their normalizations and non-asymptotic terms, and some of them still have substantial uncertainties.

All that calls for an independent estimate of the $B \rightarrow p$ form factors, which is the main goal of this paper. Here we apply a different version of LCSRs, where the roles of the final proton and initial B -meson in the underlying correlation function are inverted, as compared to the sum rules based on nucleon DAs. We use a vacuum-to- B correlation function of two local operators, one of them being the three-quark current interpolating the proton and the other one is the operator of the effective Ψ -triquark interaction. Accordingly, the nonperturbative input in the OPE for this correlation function is represented by a set of B -meson DAs [13] defined in heavy quark effective theory (HQET). The twist expansion of these DAs was elaborated in [14]. Previously, this method was applied to various B -meson transitions to light mesons (see e.g. [15, 16, 17]) as well as

to $B \rightarrow D^{(*)}$ form factors [18]. For a recent review and comparison with other versions of LCSRs see also [19].

The main advantage of the method based on B -meson DAs is a straightforward possibility to access various $B \rightarrow$ baryon form factors, replacing the proton interpolation current by any other three-quark current with a light or charmed baryon quantum numbers, while the main nonperturbative input remains the same. This allows one to obtain the form factors corresponding to different flavour structures of the effective three-quark- Ψ interaction in the mesogenesis models. In this paper, we confine ourselves to the proton mode; the others will be considered elsewhere.

Our main results are the $B \rightarrow p$ form factors obtained from LCSRs for both models (d) and (b) in the region $q^2 < 0$ of spacelike four-momentum transfer q . These form factors are then extrapolated to positive values of $q^2 = m_\Psi^2$ in the whole region of Ψ masses allowed by the mesogenesis scenario. We finally predict the $B^+ \rightarrow p\Psi$ decay branching fraction as a function of the Ψ mass. For these estimates we adopt, for definiteness, the Ψ -triquark couplings equal to their upper limits inferred in [2] from the LHC searches for new heavy particles.

In addition, we use the results of [20, 21], where, applying the heavy quark expansion method, the width of inclusive decay $B \rightarrow X_N\Psi$ was obtained in the same models (d) and (b). Here X_N denotes the sum over all kinematically accessible hadronic states generated by fragmentation of the partonic final state, formed by the diquark ud of the effective Ψ -triquark interaction and by the spectator u -quark of B^+ -meson. Dividing our new estimates of $B^+ \rightarrow p\Psi$ branching fractions to the corresponding inclusive widths, we obtain their ratios in which the unknown Ψ -triquark coupling is canceled. The inclusive invisible B decays cannot be experimentally searched for. Importantly, however, there is a theory-motivated estimate [1, 2] of the minimal inclusive width, necessary for the realization of the B -mesogenesis scenario. We use that bound, together with the estimated exclusive-to-inclusive ratios and obtain the corresponding lower limits on the exclusive $B^+ \rightarrow p\Psi$ branching fraction, which only depend on the Ψ mass and on the model of Ψ -triquark interaction. The limits we obtain are then confronted with the upper bounds measured by BaBar and Belle/Belle II.

The paper is organized as follows: in Section 2 we specify the effective interactions emerging in the considered models of B -mesogenesis. In Section 3 we derive the new LCSRs for the $B \rightarrow p$ form factors and in Section 4 we present and discuss the results of light-cone OPE in terms of B -meson DAs. Section 5 contains our numerical results. After specifying the input parameters, we present the form factors calculated from LCSRs at spacelike momentum transfer. Employing z -expansion, these form factors are continued to the physical values of Ψ mass, yielding our results for the $B \rightarrow p\Psi$ width. In Section 6 we use these results to obtain the ratios of exclusive and inclusive widths. Our concluding discussion is in Section 7. Appendix A contains the details of B -meson DAs and in Appendix B we present a derivation of the dispersion representation for logarithmic terms in the OPE.

2. The effective couplings and $B^+ \rightarrow p\Psi$ decay amplitude

For the effective Hamiltonian of the Ψ -triquark interaction generating the $B^+ \rightarrow p\Psi$ decay and its charge conjugate mode, we use the same compact form as in [10]:

$$\mathcal{H}_{(-1/3)} = -G_{(d)}\bar{\mathcal{O}}_{(d)}\Psi^c - G_{(d)}^*\bar{\Psi}^c\mathcal{O}_{(d)} + \{d \leftrightarrow b\}, \quad (1)$$

where $G_{(d)}$ is the effective four-fermion coupling, inversely proportional to the squared mass of the heavy mediator particle in the B -mesogenesis scenario (see [1, 2] for details). The local three-quark operator and its conjugate in (1) are

$$\bar{\mathcal{O}}_{(d)} = i\epsilon_{ijk}(\bar{u}_R^i b_R^{cj})\bar{d}_R^k, \quad \mathcal{O}_{(d)} = i\epsilon_{ijk}d_R^i(\bar{b}_R^{cj}u_R^k). \quad (2)$$

In the above equation, the index c (R) indicates charge conjugated (right-handed) fields, so that $q_R = \frac{1}{2}(1 + \gamma_5)q$; and i, j, k are the colour indices. The index (d) indicates the terms in the effective Hamiltonian (1) originating from the d -quark coupling to the Ψ and heavy mediator fields, that is model (d) . Replacing $d \leftrightarrow b$ yields model (b) , which corresponds to the terms in (1) with the effective coupling $G_{(b)}$ and with the three-quark operators

$$\bar{\mathcal{O}}_{(b)} = i\epsilon_{ijk}(\bar{u}_R^i d_R^{cj})\bar{b}_R^k, \quad \mathcal{O}_{(b)} = i\epsilon_{ijk}b_R^i(\bar{d}_R^{cj}u_R^k). \quad (3)$$

Considering as our main study case model (d) , we write down the amplitude of the $B^+ \rightarrow p\Psi$ decay generated by the effective operator $\bar{\mathcal{O}}_{(d)}$:

$$\mathcal{A}_{(d)}(B^+ \rightarrow p\Psi) = G_{(d)}\langle p(P)|\bar{\mathcal{O}}_{(d)}|B^+(P+q)\rangle u_{\Psi}^c(q), \quad (4)$$

where u_{Ψ}^c is the (charge conjugated) bispinor of the Ψ field, and the following on-shell conditions are fulfilled: $P^2 = m_p^2$, $(P+q)^2 = m_B^2$, $q^2 = m_{\Psi}^2$.

The hadronic matrix element of the three-quark operator in (4) can be parameterized, in the most general form, in terms of four independent $B \rightarrow p$ form factors:

$$\begin{aligned} \langle p(P)|\bar{\mathcal{O}}_{(d)}|B^+(P+q)\rangle &= F_{B \rightarrow pR}^{(d)}(q^2)\bar{u}_{pR}(P) + F_{B \rightarrow pL}^{(d)}(q^2)\bar{u}_{pL}(P) \\ &+ \tilde{F}_{B \rightarrow pR}^{(d)}(q^2)\bar{u}_{pR}(P)\frac{\not{q}}{m_p} + \tilde{F}_{B \rightarrow pL}^{(d)}(q^2)\bar{u}_{pL}(P)\frac{\not{q}}{m_p}, \end{aligned} \quad (5)$$

where $u_{pR(L)}(P) \equiv \gamma_{R(L)}u_p(P)$ and $\bar{u}_{pR(L)} \equiv \bar{u}_p(P)\gamma_{L(R)}$ are the bispinor of the right-handed (left-handed) proton and its Dirac-conjugate. Hereafter we use a compact notation:

$$\gamma_R \equiv \frac{1}{2}(1 + \gamma_5), \quad \gamma_L \equiv \frac{1}{2}(1 - \gamma_5).$$

The general expansion in terms of four form factors in (5) corresponds to the four independent kinematical structures that can be constructed using a bispinor and two independent four-momenta P and q . Note that the structures $\bar{u}_{pL,R}(P)\not{q}$ are reduced to $\bar{u}_{pL,R}(P)$ after applying the Dirac equation for bispinors. For model (b) , the same decay amplitude and its decomposition in terms of four form factors are simply obtained from (4) and (5), respectively, by the replacement $(d) \rightarrow (b)$.

3. LCSR with B -meson distribution amplitudes

Here we derive the LCSRs for the $B \rightarrow p$ form factors. For definiteness, we first consider model (d) with the three-quark operator $\overline{\mathcal{O}}_{(d)}$ specified in (2). The key element of our method is the correlation function

$$\mathcal{F}^{(d)}(P, q) = i \int d^4x e^{iP \cdot x} \langle 0 | T \{ \eta_p(x), \overline{\mathcal{O}}_{(d)}(0) \} | B^+(P + q) \rangle. \quad (6)$$

It contains the time-ordered product of $\overline{\mathcal{O}}_{(d)}$ and the proton interpolating current η_p , for which we choose the Ioffe current [22], known to be an optimal choice for other QCD sum rules in the nucleon channel:

$$\eta_p(x) = \epsilon_{ijk} [u^{Ti}(x) C \gamma^\mu u^j(x)] \gamma_5 \gamma_\mu d^k(x), \quad (7)$$

where the color indices are shown explicitly and C is the charge conjugation matrix. In our convention $C = \gamma^2 \gamma^0$. The bilocal operator product in (6) is sandwiched between the on-shell B -meson state and the vacuum.

The correlation function (6) is by construction a Dirac matrix, which is Lorentz-contracted with the two independent four-momenta P and q . Its generic decomposition in the kinematical structures reads:

$$\begin{aligned} \mathcal{F}^{(d)}(P, q) = & \left[\mathcal{F}_1^{(d)}(P^2, q^2) + \mathcal{F}_2^{(d)}(P^2, q^2) \frac{\not{P}}{m_B} + \mathcal{F}_3^{(d)}(P^2, q^2) \frac{\not{q}}{m_B} + \mathcal{F}_4^{(d)}(P^2, q^2) \frac{\not{P}\not{q}}{m_B^2} \right] \gamma_L \\ & + \left[\mathcal{F}_5^{(d)}(P^2, q^2) + \mathcal{F}_6^{(d)}(P^2, q^2) \frac{\not{P}}{m_B} + \mathcal{F}_7^{(d)}(P^2, q^2) \frac{\not{q}}{m_B} + \mathcal{F}_8^{(d)}(P^2, q^2) \frac{\not{P}\not{q}}{m_B^2} \right] \gamma_R, \end{aligned} \quad (8)$$

where $\mathcal{F}_{1,\dots,8}^{(d)}$ are Lorentz-invariant amplitudes depending on the invariant variables P^2 and q^2 .

To access the $B^+ \rightarrow p$ form factors, we employ the unitarity relation, expressing the imaginary part of the correlation function (6) in the timelike region $P^2 > 0$ of the variable P^2 , via the sum of all possible intermediate hadronic states with the quantum numbers of the interpolating current. We have:

$$\begin{aligned} \frac{1}{\pi} \text{Im} \mathcal{F}^{(d)}(P, q) = & \delta(P^2 - m_p^2) \langle 0 | \eta_p | \overline{p^+}(P) \rangle \langle \overline{p^+}(P) | \overline{\mathcal{O}}_{(d)} | B^+(P + q) \rangle \\ & + \delta(P^2 - m_{N^*}^2) \langle 0 | \eta_p | \overline{N^{*+}}(P) \rangle \langle \overline{N^{*+}}(P) | \overline{\mathcal{O}}_{(d)} | B^+(P + q) \rangle + \rho_h^{(d)}(P, q), \end{aligned} \quad (9)$$

where the overlines indicate summing over baryon polarizations. Above, we take into account that the current (7) interpolates baryons with both positive and negative P -parities. Hence, in addition to the proton contribution, we also isolate the contribution of $N^* \equiv N(1535)$, the lowest nucleon resonance with spin-parity $J^P = 1/2^-$, see [23]. Resonances and continuum states with quantum numbers $J^P = 1/2^+$ ($J^P = 1/2^-$) and heavier than the proton (the N^*) are, by default, included in the spectral density $\rho_h^{(d)}(P, q)$.

We define the hadronic matrix elements of interpolation current via the proton and N^* decay constants:

$$\langle 0 | \eta_p | p(P) \rangle = \lambda_p m_p u_p(P), \quad \langle 0 | \eta_p | N^{*+}(P) \rangle = \lambda_{N^*} m_{N^*} \gamma_5 u_{N^*}(P), \quad (10)$$

where u_p (u_{N^*}) is the Dirac bispinor for the proton (N^*) state with four-momentum P . The decay constants λ_{p,N^*} are obtained from two-point QCD sum rules or computed in lattice QCD.

Apart from the definition (5), we also need an analogous expansion of the $B \rightarrow N^*$ hadronic matrix element in terms of corresponding form factors:

$$\begin{aligned} \langle N^*(P) | \bar{\mathcal{O}}_{(d)} | B^+(P+q) \rangle &= F_{B \rightarrow N_R^*}^{(d)}(q^2) \bar{u}_{N^*R}(P) \gamma_5 + F_{B \rightarrow N_L^*}^{(d)}(q^2) \bar{u}_{N^*L}(P) \gamma_5 \\ &+ \tilde{F}_{B \rightarrow N_R^*}^{(d)}(q^2) \bar{u}_{N^*R}(P) \gamma_5 \frac{\not{q}}{m_{N^*}} + \tilde{F}_{B \rightarrow N_L^*}^{(d)}(q^2) \bar{u}_{N^*L}(P) \gamma_5 \frac{\not{q}}{m_{N^*}}, \end{aligned} \quad (11)$$

Substituting (5), (10) and (11) in (9) and summing over polarizations, we obtain

$$\begin{aligned} \frac{1}{\pi} \text{Im } \mathcal{F}^{(d)}(P, q) &= \delta(P^2 - m_p^2) \lambda_p m_p \left\{ F_{B \rightarrow pR}^{(d)}(q^2) (\not{P} + m_p) \gamma_L + F_{B \rightarrow pL}^{(d)}(q^2) (\not{P} + m_p) \gamma_R \right. \\ &\quad \left. + \tilde{F}_{B \rightarrow pR}^{(d)}(q^2) (\not{P} + m_p) \frac{\not{q}}{m_p} \gamma_R + \tilde{F}_{B \rightarrow pL}^{(d)}(q^2) (\not{P} + m_p) \frac{\not{q}}{m_p} \gamma_L \right\} \\ &- \delta(P^2 - m_{N^*}^2) \lambda_{N^*} m_{N^*} \left\{ F_{B \rightarrow N_R^*}^{(d)}(q^2) (\not{P} - m_{N^*}) \gamma_L + F_{B \rightarrow N_L^*}^{(d)}(q^2) (\not{P} - m_{N^*}) \gamma_R \right. \\ &\quad \left. + \tilde{F}_{B \rightarrow N_R^*}^{(d)}(q^2) (\not{P} - m_{N^*}) \frac{\not{q}}{m_{N^*}} \gamma_R + \tilde{F}_{B \rightarrow N_L^*}^{(d)}(q^2) (\not{P} - m_{N^*}) \frac{\not{q}}{m_{N^*}} \gamma_L \right\} + \rho^{(d)}(P, q), \end{aligned} \quad (12)$$

where it is easy to identify the kinematical structures multiplying various form factors with the ones in the decomposition (8). In general, the spectral density $\rho^{(d)}(P, q)$ is also decomposed in eight Lorentz-invariant functions:

$$\begin{aligned} \rho^{(d)}(P, q) &= [\rho_1^{(d)}(P^2, q^2) + \rho_2^{(d)}(P^2, q^2) \frac{\not{P}}{m_B} + \rho_3^{(d)}(P^2, q^2) \frac{\not{q}}{m_B} + \rho_4^{(d)}(P^2, q^2) \frac{\not{P} \not{q}}{m_B^2}] \gamma_L \\ &+ [\rho_5^{(d)}(P^2, q^2) + \rho_6^{(d)}(P^2, q^2) \frac{\not{P}}{m_B} + \rho_7^{(d)}(P^2, q^2) \frac{\not{q}}{m_B} + \rho_8^{(d)}(P^2, q^2) \frac{\not{P} \not{q}}{m_B^2}] \gamma_R. \end{aligned} \quad (13)$$

The imaginary part (12) of the correlation function enters the dispersion relation for this function in the variable P^2 at fixed q^2 ¹:

$$\mathcal{F}^{(d)}(P, q) = \frac{1}{\pi} \int_{m_p^2}^{\infty} ds \frac{\text{Im } \mathcal{F}^{(d)}(P, q)}{s - P^2}. \quad (14)$$

¹In (14), we ignore possible subtraction terms, since later they will be eliminated by the Borel transform.

We substitute the decompositions (8) and (12),(13) into the left-hand side and, respectively, right-hand side of the above relation. Equating the coefficients at each independent kinematical structure on both sides, we obtain separate dispersion relations for the eight independent invariant amplitudes. For the first four amplitudes these relations read:

$$\mathcal{F}_1^{(d)}(P^2, q^2) = \frac{\lambda_p m_p^2}{m_p^2 - P^2} F_{B \rightarrow pR}^{(d)}(q^2) + \frac{\lambda_{N^*} m_{N^*}^2}{m_{N^*}^2 - P^2} F_{B \rightarrow N_R^*}^{(d)}(q^2) + \int_{s_h}^{\infty} ds \frac{\rho_1^{(d)}(s, q^2)}{s - P^2}, \quad (15)$$

$$\mathcal{F}_2^{(d)}(P^2, q^2) = \frac{\lambda_p m_p m_B}{m_p^2 - P^2} F_{B \rightarrow pR}^{(d)}(q^2) - \frac{\lambda_{N^*} m_{N^*} m_B}{m_{N^*}^2 - P^2} F_{B \rightarrow N_R^*}^{(d)}(q^2) + \int_{s_h}^{\infty} ds \frac{\rho_2^{(d)}(s, q^2)}{s - P^2}, \quad (16)$$

$$\mathcal{F}_3^{(d)}(P^2, q^2) = \frac{\lambda_p m_p m_B}{m_p^2 - P^2} \tilde{F}_{B \rightarrow pL}^{(d)}(q^2) + \frac{\lambda_{N^*} m_{N^*} m_B}{m_{N^*}^2 - P^2} \tilde{F}_{B \rightarrow N_L^*}^{(d)}(q^2) + \int_{s_h}^{\infty} ds \frac{\rho_3^{(d)}(s, q^2)}{s - P^2}, \quad (17)$$

$$\mathcal{F}_4^{(d)}(P^2, q^2) = \frac{\lambda_p m_B^2}{m_p^2 - P^2} \tilde{F}_{B \rightarrow pL}^{(d)}(q^2) - \frac{\lambda_{N^*} m_B^2}{m_{N^*}^2 - P^2} \tilde{F}_{B \rightarrow N_L^*}^{(d)}(q^2) + \int_{s_h}^{\infty} ds \frac{\rho_4^{(d)}(s, q^2)}{s - P^2}. \quad (18)$$

The four remaining relations for the invariant amplitudes $\mathcal{F}_{5,6,7,8}^{(2)}$ are obtained from the above four equations by the following replacements of indices: in Eq. (15): $1 \rightarrow 5$, $R \rightarrow L$; in Eq. (16): $2 \rightarrow 6$, $R \rightarrow L$; in Eq. (17): $3 \rightarrow 7$, $L \rightarrow R$; in Eq. (18): $4 \rightarrow 8$, $L \rightarrow R$. The lower limit s_h in the integrals over heavier than proton continuum states is the same in all dispersion relations: $s_h = (m_p + m_{\pi^0})^2$. It corresponds to the lowest possible threshold of the positively charged pion-nucleon state with $J = 1/2$.

Below, we will calculate the correlation function (6), employing the light-cone OPE in terms of the B -meson DAs. The OPE is applicable at spacelike P^2 , such that $|P^2| \gg \Lambda_{QCD}^2$, far below the position of the proton pole at $P^2 = m_p^2$. This condition will be satisfied after Borel transform, choosing the Borel mass parameter sufficiently large. Simultaneously, the variable q^2 has to be chosen also far from respective hadronic states in the bud channel with the quantum numbers of Λ_b . Keeping $q^2 < 0$ is then sufficient. Our results for all invariant amplitudes in the region of OPE validity will be cast in a convenient form of a dispersion relations in the P^2 variable :

$$\mathcal{F}_n^{(d)OPE}(P^2, q^2) = \frac{1}{\pi} \int_0^{\infty} ds \frac{\text{Im} \mathcal{F}_n^{(d)OPE}(s, q^2)}{s - P^2}, \quad (n = 1, \dots, 8) \quad (19)$$

where the lower limit corresponds to the adopted approximation of massless u, d quarks in the OPE of the correlation function. The representation (19) allows us to employ the usual assumption of (semi-global) quark-hadron duality:

$$\int_{s_h}^{\infty} ds \frac{\rho_n^{(d)}(s, q^2)}{s - P^2} = \frac{1}{\pi} \int_{s_0(n)}^{\infty} ds \frac{\text{Im} \mathcal{F}_n^{(d)OPE}(s, q^2)}{s - P^2}, \quad (n = 1, \dots, 8) \quad (20)$$

introducing the effective threshold $s_{0(n)}$, which is in general a specific parameter for each invariant amplitude $\mathcal{F}_n^{(d)}$, hence the index (n) .

We substitute (19) into the left-hand side and, respectively, (20) into the right-hand side of each dispersion relation in (15)–(18) and their counterparts for the invariant amplitudes $\mathcal{F}_{5-8}^{(2)}$. After that, we subtract from both sides the integrals over OPE spectral densities from $s_{0(n)}$ to ∞ . Performing then the Borel transform $P^2 \rightarrow M^2$, we obtain a set of eight LCSRs containing all $B \rightarrow p$ and $B \rightarrow N^*$ form factors. The first four sum rules obtained from (15)–(18) are:

$$\begin{aligned} \lambda_p m_p^2 e^{-\frac{m_p^2}{M^2}} F_{B \rightarrow p_R}^{(d)}(q^2) + \lambda_{N^*} m_{N^*}^2 e^{-\frac{m_{N^*}^2}{M^2}} F_{B \rightarrow N_R^*}^{(d)}(q^2) \\ = \frac{1}{\pi} \int_0^{s_{0(1)}} ds e^{-\frac{s}{M^2}} \text{Im} \mathcal{F}_1^{(d)OPE}(s, q^2), \end{aligned} \quad (21)$$

$$\begin{aligned} \lambda_p m_p m_B e^{-\frac{m_p^2}{M^2}} F_{B \rightarrow p_R}^{(d)}(q^2) - \lambda_{N^*} m_{N^*} m_B e^{-\frac{m_{N^*}^2}{M^2}} F_{B \rightarrow N_R^*}^{(d)}(q^2) \\ = \frac{1}{\pi} \int_0^{s_{0(2)}} ds e^{-\frac{s}{M^2}} \text{Im} \mathcal{F}_2^{(d)OPE}(s, q^2), \end{aligned} \quad (22)$$

$$\begin{aligned} \lambda_p m_p m_B e^{-\frac{m_p^2}{M^2}} \tilde{F}_{B \rightarrow p_L}^{(d)}(q^2) + \lambda_{N^*} m_{N^*} m_B e^{-\frac{m_{N^*}^2}{M^2}} \tilde{F}_{B \rightarrow N_L^*}^{(d)}(q^2) \\ = \frac{1}{\pi} \int_0^{s_{0(3)}} ds e^{-\frac{s}{M^2}} \text{Im} \mathcal{F}_3^{(d)OPE}(s, q^2), \end{aligned} \quad (23)$$

$$\begin{aligned} \lambda_p m_B^2 e^{-\frac{m_p^2}{M^2}} \tilde{F}_{B \rightarrow p_L}^{(d)}(q^2) - \lambda_{N^*} m_B^2 e^{-\frac{m_{N^*}^2}{M^2}} \tilde{F}_{B \rightarrow N_L^*}^{(d)}(q^2) \\ = \frac{1}{\pi} \int_0^{s_{0(4)}} ds e^{-\frac{s}{M^2}} \text{Im} \mathcal{F}_4^{(d)OPE}(s, q^2). \end{aligned} \quad (24)$$

It is easy to obtain analogous sum rules for the amplitudes $\mathcal{F}_{5-8}^{(d)}$, applying to the above equations the replacements described after (18). The analogous sum rules for model (b) have the same expressions, as the ones for model (d), only the index $(d) \rightarrow (b)$ should be replaced at the form factors and OPE amplitudes.

The LCSRs derived above can now be used to estimate the $B \rightarrow p$ and, in principle, also the $B \rightarrow N^*$ form factors, provided the OPE amplitudes entering these sum rules via their spectral densities are obtained with a certain accuracy. For the channel of nucleon current, there is however an ambiguity in the separation of hadronic states into the two lowest resonances and a duality-approximated sum over excited and continuum

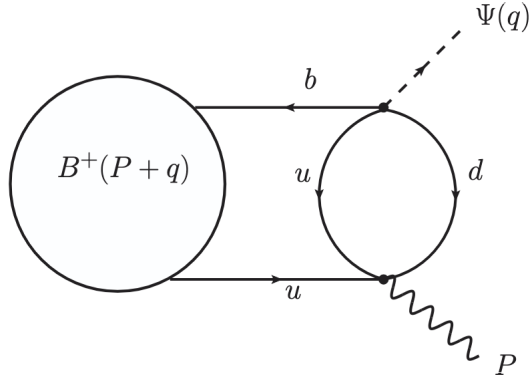


Figure 1: Diagram corresponding to the contribution of two-particle B -meson DAs to the correlation function (6). The wavy (dashed) line represents the interpolating current of the proton (the dark antibaryon).

states. A prominent and very broad Roper resonance $N(1440)$ with the same spin-parity $J^P = 1/2^+$ as the nucleon is located below $N^*(1535)$ [23]. Hence, for completeness, in each of the LCSRs (21)–(24) a $N(1440)$ contribution should be then added as a separate term proportional to a $B \rightarrow N(1440)$ form factor. The expressions for these terms are simply obtained by replacing in the proton term $p \rightarrow N(1440)$. A separate issue, which we do not discuss here, concerns accounting for the large total widths of N^* and $N(1440)$ in the resonance-pole terms.

Disentangling the $B \rightarrow p$ form factors from sum rules that contain two additional resonance terms would require a dedicated fit procedure, for which the knowledge of all three decay constants λ_p , λ_{N^*} and $\lambda_{N(1440)}$ is necessary. However, we are unaware of any reliable estimate of the $N(1440)$ decay constant. Hence, in our numerical analysis performed below, we leave such a separation procedure beyond our scope. Instead, we employ a simplified form of the hadronic part, following previous analyses of LCSRs for the nucleon electromagnetic form factors (see e.g., [24, 25]). In those sum rules the same proton (nucleon) interpolating current was used and the nucleon resonances $N(1440)$ and $N^*(1535)$ were incorporated into the spectral density $\rho_n^{(d)}(s)$ via the duality approximation (20), where the effective threshold $s_{0(n)}$ was adjusted accordingly.

We now turn to the OPE of the correlation function (6), aiming at the OPE spectral density that enters LCSRs.

4. OPE for the correlation function

4.1. Contribution of two-particle DAs

To describe the calculation of the correlation function in detail, we take, for definiteness, model (d) and substitute in (6) the expression (2) for the operator $\overline{\mathcal{O}}_{(d)}$ in terms of quark fields. Contracting the u and d fields in the free massless-quark propagators, we

encounter the leading-order (LO) diagram depicted in Fig. 1. At this level, due to the presence of three-quark currents, the diagram already contains a diquark loop ².

The remaining matrix element in the expression for the LO diagram is the product of \bar{b} - and u -quark fields at points 0 and x , respectively, sandwiched between the B^+ -meson and vacuum states. For that matrix element, we employ the HQET limit, replacing \bar{b} field by an effective \bar{h}_v field and use the expansion in terms of B -meson DAs. Their definitions, twist assignment and dependence on the momentum variable are presented in Appendix A. Here the index v indicates the velocity four-vector $v = (P + q)/m_B$. We arrive at the following intermediate expression for the OPE of the correlation function:

$$\begin{aligned} \mathcal{F}^{(d)OPE}(P, q) &= 2 \left(\frac{if_B m_B}{8} \right) \int_0^\infty d\omega \int d^4x e^{i(P-\omega v) \cdot x} \frac{x_\alpha x_\beta}{(2\pi^2)^2 (x^2)^4} \\ &\times \left\{ -\text{Tr}[\gamma^\mu \gamma^\alpha (1 + \not{v})] \phi_+^B(\omega) + \text{Tr}[\gamma^\mu \gamma^\alpha (1 + \not{v}) \not{x}] \frac{i}{2} \Phi_\pm^B(\omega) \right\} \gamma_5 \gamma_\mu \gamma_\beta (1 + \not{v}) + \dots \end{aligned} \quad (25)$$

where for brevity we only show the contributions of the twist-2 and twist-3 DAs. Note that a factor of 2 is inserted in the above to account for the two possible contractions of the u -quark fields in (6), leading to equal results. Performing the Dirac-matrix algebra and integrating over the four-coordinate x , we finally obtain:

$$\begin{aligned} \mathcal{F}^{(d)OPE}(P, q) &= \frac{f_B m_B}{16\pi^2} \int_0^\infty d\omega \left[(P - \omega v)^2 \ln[-(P - \omega v)^2] \phi_+^B(\omega) \right. \\ &\quad - \ln[-(P - \omega v)^2] (\not{P} \not{v} - \omega) \Phi_\pm^B(\omega) \\ &\quad \left. - 8 \ln[-(P - \omega v)^2] g_+^B(\omega) + 8 \frac{(\not{P} \not{v} - \omega)}{(P - \omega v)^2} G_\pm^B(\omega) \right] \gamma_L, \end{aligned} \quad (26)$$

where also the twist-4 and twist-5 DAs contribute. Note that after the x -integration in (25) only the (convergent at $D = 4$) terms generating imaginary part over the variable P^2 are retained in (26), whereas the constant and polynomial terms in P^2 are omitted, since they will vanish after Borel transform.

Following the same procedures as before, we calculate the correlation function in model (b), and obtain a simple relation:

$$\mathcal{F}^{(b)OPE}(P, q) = 2\mathcal{F}^{(d)OPE}(P, q). \quad (27)$$

Matching the result of our calculation in (26) with the decomposition (8), we find that only the invariant amplitudes $F_1^{(d)}(P^2, q^2)$ and $F_4^{(d)}(P^2, q^2)$ contribute to the adopted approximation of OPE. We also make the dependence on the momentum squared P^2 explicit, transforming:

$$-(P - \omega v)^2 = \left(1 - \frac{\omega}{m_B} \right) (s(\omega) - P^2), \quad (28)$$

²Note that in previous applications of the LCSRs with B -meson DAs to the $B \rightarrow$ meson form factors, the hard-scattering part of LO diagrams represents a single virtual quark line connecting two vertices of currents.

where a new variable

$$s(\omega) = \frac{\omega[m_B(m_B - \omega) - q^2]}{m_B - \omega} \quad (29)$$

is introduced, so that $s(0) = 0$, $s(\infty) = \infty$ (with the asymptotic behavior $\lim_{\omega \rightarrow \infty} s(\omega) \sim m_B \omega$) and, inversely:

$$\omega(s) = \frac{1}{2m_B} \left(m_B^2 - q^2 + s - \sqrt{(m_B^2 - q^2 + s)^2 - 4m_B^2 s} \right). \quad (30)$$

Furthermore, since we are only interested in the terms in the expression (26) that develop imaginary part in the variable P^2 , we use (28) and replace

$$\ln[-(P - \omega v)^2] \rightarrow \ln[s(\omega) - P^2].$$

The resulting invariant amplitudes in the decomposition (8) are:

$$\begin{aligned} \mathcal{F}_1^{(d)OPE}(P^2, q^2) = & \frac{f_B}{16\pi^2} \int_0^\infty d\omega \left[- (m_B - \omega)(s(\omega) - P^2) \ln[s(\omega) - P^2] \phi_+^B(\omega) \right. \\ & - \ln[s(\omega) - P^2] (P^2 - \omega m_B) \Phi_\pm^B(\omega) \\ & \left. - 8m_B \ln[s(\omega) - P^2] g_+^B(\omega) - \frac{8(s(\omega) - \omega m_B)}{\left(1 - \frac{\omega}{m_B}\right)(s(\omega) - P^2)} G_\pm^B(\omega) \right], \quad (31) \end{aligned}$$

where, in the coefficient multiplying G_\pm^B , the term that does not contribute to the imaginary part is removed, replacing $P^2 \rightarrow s(\omega)$ in the numerator, and

$$\mathcal{F}_4^{(d)OPE}(P^2, q^2) = \frac{f_B m_B^2}{16\pi^2} \int_0^\infty d\omega \left[- \ln[s(\omega) - P^2] \Phi_\pm^B(\omega) - \frac{8G_\pm^B(\omega)}{\left(1 - \frac{\omega}{m_B}\right)(s(\omega) - P^2)} \right]. \quad (32)$$

All remaining invariant amplitudes vanish, that is $\mathcal{F}_{2,3}^{(d)}(P^2, q^2) = \mathcal{F}_{5,6,7,8}^{(d)}(P^2, q^2) = 0$ in the adopted LO and twist-5 approximation³.

The next task is to transform (31) and (32) to the form of a dispersion integral (19). The details of that procedure are explained in Appendix B. Applying it, we calculate the imaginary parts of the invariant amplitudes entering the integrals on right-hand sides of the LCSRs (21) and (24):

$$\begin{aligned} \text{Im} \mathcal{F}_1^{(d)OPE}(s, q^2) = & \frac{f_B}{16\pi} \left\{ \int_0^{\omega(s)} d\omega' \left[\left(\omega' [m_B(m_B - \omega') - q^2] - (m_B - \omega')s \right) \phi_+^B(\omega') \right. \right. \\ & \left. \left. + (s - m_B \omega') \Phi_\pm^B(\omega') + 8m_B g_+^B(\omega') \right] - \frac{8m_B(s - m_B \omega(s))}{m_B - \omega(s)} \frac{d\omega(s)}{ds} G_\pm^B(\omega(s)) \right\}, \quad (33) \end{aligned}$$

³Since the amplitudes $\mathcal{F}_{5,6,7,8}^{(d)}$ belong to the Dirac structures with γ_R in the decomposition (8), we expect that their absence is not related to the accuracy of OPE, but is rather correlated with the chirality properties of the underlying operator $\bar{O}_{(d)}$. This conjecture deserves further investigation which is beyond our scope here.

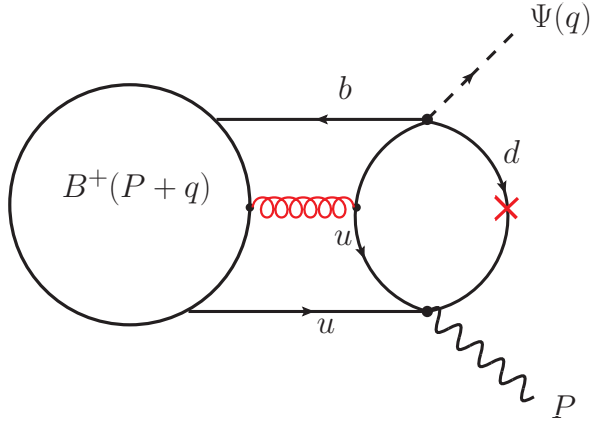


Figure 2: Diagram describing the contributions of three-particle (quark-antiquark-gluon) B -meson DAs to the correlation function (6). The curly line represents a gluon component of the DA. The cross indicates the second diagram, where the gluon is attached to the d -quark.

$$\text{Im}\mathcal{F}_4^{(d)OPE}(s, q^2) = \frac{f_B m_B^2}{16\pi} \left\{ \int_0^{\omega(s)} d\omega' \Phi_{\pm}^B(\omega') - \frac{8m_B G_{\pm}^B(\omega(s))}{m_B - \omega(s)} \frac{d\omega(s)}{ds} \right\}, \quad (34)$$

where the q^2 -dependence of the function $\omega(s)$ defined in (30) is not shown for brevity. Note that in the adopted accuracy of OPE, the remaining contributions to these sum rules vanish:

$$\text{Im}\mathcal{F}_2^{(d)OPE}(s, q^2) = \text{Im}\mathcal{F}_3^{(d)OPE}(s, q^2) = 0.$$

4.2. Contribution of three-particle DAs

The contributions of B -meson three-particle DAs to OPE are described by the diagrams shown in Fig. 2. To compute them, we need the quark propagator expanded near the light-cone up to the first-order in gluon-field strength. In the adopted limit of massless u, d quarks, the corresponding expression reads [26]:

$$\begin{aligned} -i\langle 0|T\{q_{\alpha}^i(x) \bar{q}_{\beta}^k(0)\}|0\rangle &= \frac{\not{x}_{\alpha\beta} \delta^{ik}}{2\pi^2(-x^2)^2} \\ &+ \frac{g_s(\lambda^a)^{ik}}{32\pi^2(-x^2)} \int_0^1 du \left\{ u \sigma_{\mu\nu} G^{a\mu\nu}(ux) \not{x} + \bar{u} \not{x} \sigma_{\mu\nu} G^{a\mu\nu}(ux) \right\}_{\alpha\beta}, \end{aligned} \quad (35)$$

where λ^a are the Gell-Mann matrices and the Dirac and color indices are shown explicitly.

To obtain the contribution of the first diagram, where the gluon from the B -meson DA is attached to the virtual u -quark, we use the second term in (35), while using the free propagator for the virtual d -quark. For the second diagram, these two terms are

interchanged. As in the case of the LO diagram, the two possibilities to contract u -quark lines originating from the operator $\bar{\mathcal{O}}_{(d)}$ and interpolating current yield an overall factor of 2. The three-particle DAs that arise when the quark, antiquark, and gluon fields are sandwiched between the B -meson and vacuum states are described in Appendix A. Our result for the diagram with gluon attached to the u -quark reads:

$$\mathcal{F}_{\text{OPE}}^{(d)}(P, q)|_u = -\frac{f_B m_B}{64\pi^2} \int_0^\infty dw_1 \int_0^\infty dw_2 \int_0^1 \frac{du}{\mathcal{P}^2} \left[u \mathcal{C}(\mathcal{P}, v) + \bar{u} \bar{\mathcal{C}}(\mathcal{P}, v) \right] \gamma_L, \quad (36)$$

where $\mathcal{P} \equiv P - \sigma m_B v$, with the function $\sigma = \sigma(u, \omega_1, \omega_2)$ defined in (A.17). The lengthy expressions for the coefficients \mathcal{C} and $\bar{\mathcal{C}}$ are presented in (A.19) in Appendix A.

The calculation of the remaining diagrams yields the following relations:

$$\mathcal{F}^{(d)_{\text{OPE}}}(P, q)|_d = -\mathcal{F}^{(d)_{\text{OPE}}}(P, q)|_u, \quad (37)$$

$$\mathcal{F}^{(b)_{\text{OPE}}}(P, q)|_d = \mathcal{F}^{(b)_{\text{OPE}}}(P, q)|_u = 0. \quad (38)$$

Thus, the contribution of three-particle DAs to the correlation function vanishes for both models (d) and (b). The reason, as follows from a detailed inspection of the diagram expressions, lies in the specific Dirac structure of the chosen proton interpolating current. Note that Ioffe current is a definite linear combination of two other three-quark currents (see e.g. [27] for details). We checked that both of them produce nonvanishing contributions which then cancel or vanish in this combination. Furthermore, the Dirac structure of the effective interactions given by the operators (2) and (3) coupled to Ψ plays a role too. Note that in these interactions both diquark and quark- Ψ fields form Lorentz-scalars. If the effective interaction would have another Dirac structure, e.g., $(\bar{u}_R^i \gamma_\rho b_R^c) (\bar{d}_R \gamma^\rho \Psi)$ in model (d), (or the same with $d \leftrightarrow b$ in model (b)), the contributions of the diagrams in Fig. 2 would not vanish in both models, even in combination with the Ioffe current.

As a cross-check, we recalculated the diagrams in Fig. 2 with quark propagators in the momentum representation and in $D \neq 4$. We found that, in our case of massless u, d quarks, the same relations (37) and (38) are valid. On the other hand, replacing in the correlation function the massless d -quark by a massive s -quark (which would correspond to a decay mode $B \rightarrow \Lambda \Psi$), yields nonvanishing terms proportional to m_s for the contributions of three-particle DAs.

5. Numerical results

5.1. Inputs

In Table 1, we collect the values and intervals of all input parameters used in our numerical analysis. For LCSRs, apart from hadron masses taken from [23], we need the proton decay constant λ_p defined in (10). For that we take the interval from [28], determined from two-point QCD sum rule for the same Ioffe currents.

| Parameters | values/intervals | Source |
|--|---|------------|
| Hadron masses | $m_B = 5.279 \text{ GeV}$ $m_p = 938.272 \text{ MeV}$ $m_{\Lambda_b} = 5.620 \text{ GeV}$ $m_{\pi^+} = 139.57 \text{ MeV}$ | [23] |
| Nucleon decay constant | $\lambda_p = -(27 \pm 9) \times 10^{-3} \text{ GeV}^2$ | [28] |
| B -meson decay constant | $f_B = 190.0 \pm 1.3 \text{ MeV}$ | [29] |
| Inverse moment of tw2 B DA | $\lambda_B = 460 \pm 110 \text{ MeV}$ | [30] |
| The ratio (A.12) | $R = \lambda_E^2 / \lambda_H^2 = 0.30^{+0.17}_{-0.12}$ | see App. A |
| Borel parameter squared | $M^2 = 1.5 - 2.0 \text{ GeV}^2$ | [24] |
| Duality threshold | $s_0 = 2.25 \text{ GeV}^2$ | |
| b -quark $\overline{\text{MS}}$ mass | $\overline{m}_b(\mu = 3 \text{ GeV}) = 4.47^{+0.04}_{-0.03} \text{ GeV}$ | [23] |
| B^+ -meson lifetime | $\tau_B = 1.638 \pm 0.004 \text{ ps}$ | [23] |

Table 1: The input parameters used in the numerical analysis.

Definitions and models adopted for the B -meson DAs entering LCSRs are described in Appendix A. The whole set of these DAs contains three input parameters, which currently have different levels of precision. The B -meson decay constant is very accurately determined from lattice QCD calculations. We adopt the average of $N_f = 3 + 1 + 1$ results from [29]. Still far more uncertain is the inverse moment of the twist-2 B -meson DA defined in (A.11). We use the determination of this parameter from QCD sum rule based on local OPE [30] (see also [31]). The third input for B -meson DAs is the ratio (A.12), for which the interval in Table 1 is obtained by averaging the parameters λ_E and λ_H over three independent determinations [13], [32], [33] from QCD sum rules based on different two-point correlation functions. Adopting the values quoted in Table 1, we tacitly choose for λ_B and other scale-dependent parameters one and the same renormalization scale $\mu \sim 1 \text{ GeV}$, which lies in the ballpark of the Borel mass scale. More accurate choice of scales demands computation of gluon radiative corrections to the correlation function, which is a technically quite a demanding task remaining beyond our scope. Finally, for the estimate of the inclusive width $B \rightarrow X_N \Psi$ used below in Section 6, we use the b -quark mass from [23] at the scale $\mu = 3 \text{ GeV}$.

5.2. Numerical analysis of LCSRs

According to our results for the OPE obtained in Section 4, within the adopted approximation only the two invariant amplitudes $\mathcal{F}_1^{(d)}$ and $\mathcal{F}_4^{(d)}$ contribute to the LCSRs derived in Section 3, whereas all other amplitudes vanish. Hence, here we concentrate

on the numerical analysis of the two sum rules (21) and (24).

Furthermore, as already discussed above, we simplify the hadronic parts of these sum rules, including all nucleon resonance contributions into the part of the hadronic spectral density that is approximated with the quark-hadron duality, applying (20). In this respect, we follow the analysis of the LCSRs for the nucleon electromagnetic form factors (see e.g. [24, 25]). It is then natural to adopt the same effective threshold $s_{0(N)} \simeq (1.5 \text{ GeV})^2 = 2.25 \text{ GeV}^2$ and the same interval of Borel mass squared, $M^2 = 1.5 - 2.0 \text{ GeV}^2$.

From the LCSRs (21) and (24) we finally obtain the $B \rightarrow p$ form factors

$$F_{B \rightarrow p_R}^{(d)}(q^2) = \frac{1}{\pi \lambda_p m_p^2} \int_0^{s_{0(N)}} ds e^{\frac{m_p^2 - s}{M^2}} \text{Im} \mathcal{F}_1^{(d)OPE}(s, q^2), \quad (39)$$

$$\tilde{F}_{B \rightarrow p_L}^{(d)}(q^2) = \frac{1}{\pi \lambda_p m_B^2} \int_0^{s_{0(N)}} ds e^{\frac{m_p^2 - s}{M^2}} \text{Im} \mathcal{F}_4^{(d)OPE}(s, q^2). \quad (40)$$

We parenthetically note that the LCSRs (22) and (23) with a vanishing OPE part indicate nontrivial cancellation between the $B \rightarrow p$, $B \rightarrow N^*(1535)$ and $B \rightarrow N(1440)$ form factors, or in other words, relations between these form factors which deserve a separate study. For the form factors in model (b), we have the same LCSRs (39) and (40), where the right-hand side is multiplied by a factor 2, as implied by the relation (27). Hence:

$$F_{B \rightarrow p_R}^{(b)}(q^2) = 2F_{B \rightarrow p_R}^{(d)}(q^2), \quad \tilde{F}_{B \rightarrow p_L}^{(b)}(q^2) = 2\tilde{F}_{B \rightarrow p_L}^{(d)}(q^2). \quad (41)$$

Having at hand all input parameters, we evaluate the form factors given by the LCSRs (39) and (40) in the region of their validity, $q^2 < 0$. The numerical values of both form factors $F_{B \rightarrow p_R}^{(d)}(q^2)$ and $\tilde{F}_{B \rightarrow p_L}^{(d)}(q^2)$ at the central input and in the interval $-8.0 \text{ GeV}^2 \leq q^2 \leq 0$ are plotted in Fig. 3. To illustrate the convergence of OPE, we also display in the same figure the contributions of B -meson DAs with separate twists. Since the twist-3 DA ϕ_-^B enters LCSRs only in the integrated linear combination with the twist-2 DA ϕ_+^B , we add together their contributions. For the same reason, we plot the sum of twist-4 and twist-5 contributions. We also separately display the contribution of twist-4 DA, to assess the influence of the twist-5 term on LCSRs.

Comparing separate contributions to LCSRs, we find that for the form factor $F_{B \rightarrow p_R}^{(d)}$, across the entire q^2 interval, the DAs of higher twists 4,5 have smaller contributions than the DAs of lower twists 2,3, while the effect of adding the twist-5 DA is negligible. A similar hierarchy is observed for the form factor $\tilde{F}_{B \rightarrow p_L}^{(d)}$, however, here the twist-5 DA has a larger contribution than its twist-4 counterpart. For model (b), the identical pattern appears scaled by a factor of two, as follows from the relation (41). In addition, our numerical analysis reveals, that applying a simplified version of hadronic part with the effective threshold s_0 covering nucleon resonances affects the proportion between the proton-pole term and the integral above s_0 in the LCSRs. The pole term contribution

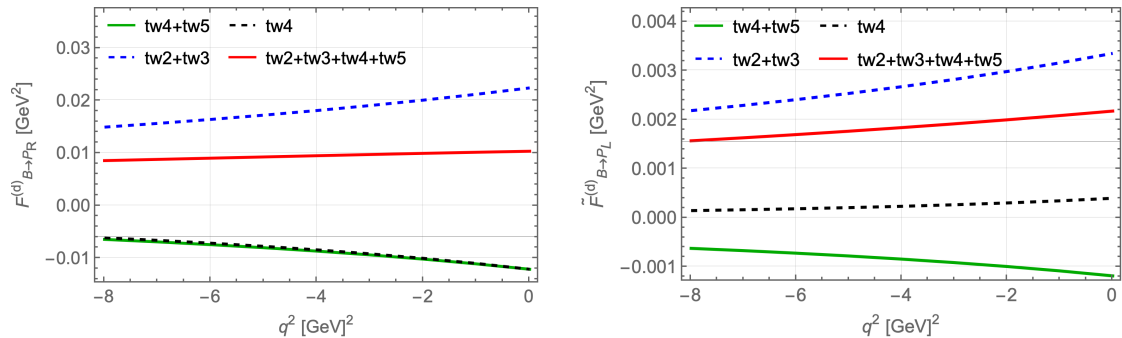


Figure 3: The form factors $F_{B \rightarrow P_R}^{(d)}$ (left panel) and $\tilde{F}_{B \rightarrow P_L}^{(d)}$ (right panel) in the spacelike region and at central input, shown with the red solid lines. The blue dashed (green solid) lines represent the sum of the twist-2 and twist-3 (twist-4 and twist-5) contributions, and the black dashed line represents the twist-4 contribution.

to the sum rule becomes subdominant, which means that the our LCSR results have a substantial reliance on the quark-hadron duality approximation.

Up to this point, the numerical evaluation of the form factors from LCSRs was done at the central values of the input parameters. We also estimate total uncertainties of our predictions arising from the variation of input parameters within adopted intervals. The uncertainties of the form factors are obtained by adding the individual parametric variations in quadrature, and by propagating the resulting upper and lower variations.

In Table 2, we present, as a sample of our results, the $B \rightarrow p$ transition form factors at $q^2 = 0$. The final results (denoted as LCSR- B) are in the column (tw2-tw5), while the column (tw2-tw3) is just for illustration. The resulting uncertainties are quite large, mainly due to the broad intervals of the two key input parameters: the inverse moment λ_B of the leading twist-2 DA, and the nucleon decay constant λ_p . Note that we prefer to display our predictions in this Table in the form of intervals, because for an LCSR numerical result no Gaussian distribution can be attributed to the most important input uncertainties. Indeed, both λ_B and λ_p are themselves derived from two-point QCD sum rules.

In the same Table, we also quote previous results for the $B \rightarrow p$ form factors obtained from LCSRs employing the nucleon DAs, denoted as LCSR- N . For the latter sum rules, the initial twist-3 accuracy in [10] was upgraded in [12] up to the twist-6 level. Comparing both methods and their results with each other, we first of all notice that the simple relations (41) between the form factors in models (d) and (b) predicted above are absent in the LCSR- N at any twist. Moreover, in the latter approach both (b)-model form factors have a different sign with respect to the ones in model (d).

We emphasize that the concept of twist for the nucleon DAs is completely different from the one used for the B -mesons DAs. Therefore, a direct one-to-one comparison of separate twist contributions obtained with both sum rule methods is pointless as such. Still, an overall suppression of larger-twist contributions remains a general criterion of

| Form factor | LCSR- B (this work) | | LCSR- N | |
|--|-----------------------|--------------|--------------|----------------|
| | (tw2-tw3) | (tw2-tw5) | (tw3) [10] | (tw3-tw6) [12] |
| $F_{B \rightarrow p_R}^{(d)}(0)$ | [1.4, 3.9] | [0.4, 2.2] | [2.4, 2.8] | [0.9, 3.5] |
| $\tilde{F}_{B \rightarrow p_L}^{(d)}(0)$ | [0.24, 0.52] | [0.14, 0.35] | 0 | [0.4, 0.7] |
| $F_{B \rightarrow p_R}^{(b)}(0)$ | [2.8, 7.7] | [0.8, 4.4] | [-0.9, -0.6] | [-5.9, -2.2] |
| $\tilde{F}_{B \rightarrow p_L}^{(b)}(0)$ | [0.5, 1.1] | [0.28, 0.70] | [0.07, 0.10] | [-0.9, -0.4] |

Table 2: Intervals of the $B \rightarrow p$ transition form factors at $q^2 = 0$ (in units of 10^{-2} GeV²) for models (d) and (b), obtained from LCSRs with B -meson DAs (denoted as LCSR- B), are compared with the results from LCSRs with nucleon DAs (LCSR- N). Here the notation such as (tw2-tw5) indicates that contributions from twist-2 up to twist-5 are included.

validity, which is also satisfied by our LCSR- B results. On the contrary, according to [12], the LCSR- N method yields large, and even dominant contributions of higher twists. To test that in more detail, we used the sum rule expressions from [12] in the spacelike region, together with the input adopted there, and compared numerical contributions from nucleon DAs of different twist. Specifically, concentrating on model (b), and taking $q^2 = -4.0$ GeV², where the twist expansion is expected to be valid, we found for the form factor $F_{B \rightarrow p_R}^{(b)}(q^2)$, that the twist-4 (twist-5) contribution is four times larger (amounts to 60%) than the twist-3 one. For the second form factor $\tilde{F}_{B \rightarrow p_L}^{(b)}(q^2)$ in the same model (b) the ratio of twist-4 to twist-3 contributions reaches an order of magnitude. This significant enhancement explains a rather large difference between the LCSR- N form factors in the first and second column of Table 2, especially for model (b). For model (d) the effects of higher twists are much less pronounced, and the agreement with our estimates is also better.

Furthermore, we also verified the resulting uncertainties of the form factors obtained in [12] and quoted as intervals in Table 2. To this end, we performed an independent Monte-Carlo study of these uncertainties and found agreement at $q^2 = 0$ with the intervals in the last column of Table 2. The fact that the latter intervals are also broad can be traced to a combination of enhanced twist-4,5 effects in the LCSR- N method with still uncertain parameters of the corresponding nucleon DAs.

Note that the estimated large uncertainties of both LCSR methods yield an effective marginal agreement between their predictions, in the form of an overlap between the intervals of predicted form factor values. But the status of OPE, expressed via hierarchy of twist contributions, remains questionable for the LCSR- N approach, at least for model (b), and deserves further investigation.

Our LCSR- B results will be used in the next subsection for extrapolation of the form factors to the physical region of the $B^+ \rightarrow p\Psi$ decay.

5.3. Branching fraction of the $B^+ \rightarrow p\Psi$ decay

The mass of the dark antibaryon Ψ in the $B^+ \rightarrow p\Psi$ decay can vary within the interval

$$m_p \simeq 0.94 \text{ GeV} < m_\Psi < (m_B - m_p) \simeq 4.21 \text{ GeV}, \quad (42)$$

where the lower limit follows from the constraint that is put in mesogenesis models [1, 2] to avoid the proton decay into Ψ . Hence, in order to estimate the width of $B^+ \rightarrow p\Psi$, we need to extrapolate the $B \rightarrow p$ form factors obtained from LCSRs at $q^2 < 0$ to the timelike region of $q^2 = m_\Psi^2$ between m_p^2 and $(m_B - m_p)^2$.

The invariant form factors determining the $B \rightarrow p$ hadronic matrix element in (5) have the same analytic properties as any other hadron form factor. The variable q^2 can be continued from the region $q^2 < 0$ to the whole complex q^2 -plane. Singularities of any $B \rightarrow p$ form factor are located on the positive real axis and are generated by intermediate hadronic states with the quantum numbers of b -baryons. The lowest singularity is the pole at $q^2 = m_{\Lambda_b}^2$ associated with the Λ_b -baryon. The next isospin-zero state is a hadronic continuum state composed from Λ_b and two pions. This state develops a branch point at $q^2 = (m_{\Lambda_b} + 2m_\pi)^2$. Without going into details on other heavier states, we only notice that the threshold corresponding to the state of B -meson and proton at $q^2 = (m_B + m_p)^2$ is by $\simeq 300$ MeV heavier than the state $\Lambda_b 2\pi$.

Taking all these comments into account, we apply to the $B \rightarrow p$ form factors a standard z -expansion method based on analyticity, which is widely used for heavy-to-light form factors and was also employed in [10] for the same $B \rightarrow p$ form factors. For definiteness, we consider the form factor $F_{B \rightarrow pR}^{(d)}(q^2)$, all others are treated in the same way. We employ the transformation of the variable q^2 to a new variable z , defined as

$$z(q^2) = \frac{\sqrt{t_+ - q^2} - \sqrt{t_+}}{\sqrt{t_+ - q^2} + \sqrt{t_+}}, \quad (43)$$

with $t_+ = (m_{\Lambda_b} + 2m_\pi)^2$. Note that, for simplicity, we put to zero the other (arbitrary) parameter t_0 of this transformation, hence the point $q^2 = 0$ transforms to $z = 0$. The spacelike interval, in which the form factor $F_{B \rightarrow pR}^{(d)}(q^2)$ and the other form factors are evaluated using LCSRs, and the physical q^2 region relevant for the $B^+ \rightarrow p\Psi$ decay are mapped, respectively, as follows:

$$-8.0 \text{ GeV}^2 < q^2 < 0 \quad \rightarrow \quad 0.083 \geq z \geq 0, \quad (44)$$

$$m_p^2 < q^2 < (m_B - m_p)^2 \quad \rightarrow \quad -0.067 > z > -0.20. \quad (45)$$

Since the lowest possible threshold ⁴ is chosen for the parameter t_+ , only the Λ_b -pole of the form factor remains within the whole region $|z| < 1$ on which the q^2 -plane maps. To remove this pole, we multiply the form factors by $(1 - q^2/m_{\Lambda_b}^2)$. The resulting function

⁴Note that in [10, 12], while using a similar z -expansion, the Bp threshold was tacitly assumed to be the lowest one, choosing $t_+ = (m_B + m_p)^2$. Here we correct this oversight. At the same time we checked that if we would adopt the same higher threshold, the numerical results for the extrapolated form factors shift within 1% from our results obtained with a correct choice.

of z , $(1 - q^2(z)/m_{\Lambda_b}^2)F_{B \rightarrow p_R}^{(d)}(q^2(z))$ is then singularity-free at $|z| < 1$. Owing to the fact that both intervals of z variable (44) and (45) are close to $z = 0$, we expand this function in the powers of z around $z = 0$ and approximate it by first few terms.

More specifically, we use the standard BCL form of the z -expansion [34], retaining terms up to $O(z^2)$. We employ a convenient form of this parametrization (see e.g., [10]):

$$F_{B \rightarrow p_R}^{(d)}(q^2) = \frac{F_{B \rightarrow p_R}^{(d)}(0)}{1 - q^2/m_{\Lambda_b}^2} \left\{ 1 + \beta_{B \rightarrow p_R}^{(d)} \left[z(q^2) - z(0) + \frac{1}{2} (z(q^2)^2 - z(0)^2) \right] \right\}. \quad (46)$$

in terms of two parameters: the form-factor value at $q^2 = 0$ and the slope parameter $\beta_{B \rightarrow p_R}^{(d)}$. A similar expression with the corresponding slope parameter $\tilde{\beta}_{B \rightarrow p_L}^{(d)}$ is used for the form factor $\tilde{F}_{B \rightarrow p_L}^{(d)}(q^2)$. For the model-(b) form factors, the relations (41) are again used, yielding

$$F_{B \rightarrow p_R}^{(b)}(0) = 2F_{B \rightarrow p_R}^{(d)}(0), \quad \tilde{F}_{B \rightarrow p_L}^{(b)}(0) = 2\tilde{F}_{B \rightarrow p_L}^{(d)}(0), \quad (47)$$

and equalities of slope parameters:

$$\beta_{B \rightarrow p_R}^{(b)} = \beta_{B \rightarrow p_R}^{(d)}, \quad \tilde{\beta}_{B \rightarrow p_L}^{(b)} = \tilde{\beta}_{B \rightarrow p_L}^{(d)}. \quad (48)$$

The next step is a fit of the parameterization (46) to our LCSR results for the form factor $F_{B \rightarrow p_R}^{(d)}(q^2)$ at $q^2 \leq 0$. To this end, we perform two different procedures. First, we take the LCSR form factor at $q^2 = 0$ as a fixed external input and fit only the single slope parameter $\beta_{B \rightarrow p_R}^{(d)}$, using the form factor calculated at eight equidistant points in the interval (44). The fit is repeated, varying the form factor within the estimated parametric uncertainty induced by the LCSR input. This variation is then propagated to determine the upper and lower limits of the slope parameter $\beta_{B \rightarrow p_R}^{(d)}$ in a form of an asymmetric error. We repeat the same fit procedure for the second form factor $\tilde{F}_{B \rightarrow p_L}^{(d)}(q^2)$. The resulting parameters of z -expansion are presented in Table 3, where for the (b)-model form factors we use the relations (47) and (48).

This simple approach with a fixed normalization and fitted slope parameter of the form factor reflects the full range of the form factor uncertainties, however the correlations between the two parameters of our z -expansion are not explicitly included in the error propagation. To assess the impact of such correlations, we have also performed an alternative fit, in which the value of $F_{B \rightarrow p_R}^{(d)}(0)$ is treated as a nuisance parameter and varied within its uncertainty. In that case, the covariance matrix obtained from the Hessian automatically accounts for correlations between the normalization and the slope. We find that the resulting branching fractions agree within uncertainties with those obtained in the fixed-normalization approach, indicating that correlation effects are inessential.

Having determined the form factors in the timelike region of $q^2 = m_{\Psi}^2$ via the z -expansion, we can now predict the branching fraction for $B^+ \rightarrow p\Psi$ as a function of the Ψ mass. The expression for the decay branching fraction in terms of the form factors

| | | | |
|--|------------------------|---|-------------------------|
| $F_{B \rightarrow p_R}^{(d)}(0)$ | $1.0_{-0.6}^{+1.2}$ | $\beta_{B \rightarrow p_R}^{(d)}$ | $0.99_{-1.4}^{+3.4}$ |
| $\tilde{F}_{B \rightarrow p_L}^{(d)}(0)$ | $0.22_{-0.08}^{+0.13}$ | $\tilde{\beta}_{B \rightarrow p_L}^{(d)}$ | $-1.78_{-0.17}^{+0.76}$ |
| $F_{B \rightarrow p_R}^{(b)}(0)$ | $2.0_{-1.2}^{+2.4}$ | $\beta_{B \rightarrow p_R}^{(b)}$ | $0.99_{-1.4}^{+3.4}$ |
| $\tilde{F}_{B \rightarrow p_L}^{(b)}(0)$ | $0.44_{-0.16}^{+0.26}$ | $\tilde{\beta}_{B \rightarrow p_L}^{(b)}$ | $-1.78_{-0.17}^{+0.76}$ |

Table 3: Parameters of the z -expansion (46) obtained from the fit of LCSRs. Presented are the $B \rightarrow p$ form factors at $q^2 = 0$ (in units of 10^{-2} GeV²) and the dimensionless slope parameters.

was already given in [10], e.g., we have for model (d):

$$\text{BR}_{(d)}(B^+ \rightarrow p\Psi) = |G_{(d)}|^2 \left\{ \left[\left(F_{B \rightarrow p_R}^{(d)}(m_\Psi^2) \right)^2 + \frac{m_\Psi^2}{m_p^2} \left(\tilde{F}_{B \rightarrow p_L}^{(d)}(m_\Psi^2) \right)^2 \right] (m_B^2 - m_p^2 - m_\Psi^2) + 2m_\Psi^2 F_{B \rightarrow p_R}^{(d)}(m_\Psi^2) \tilde{F}_{B \rightarrow p_L}^{(d)}(m_\Psi^2) \right\} \frac{\lambda^{1/2}(m_B^2, m_p^2, m_\Psi^2)}{16\pi m_B^3} \tau_{B^+}, \quad (49)$$

where $\lambda(a, b, c) = a^2 + b^2 + c^2 - 2ab - 2ac - 2bc$ is the Källén function and τ_{B^+} is the B^+ -meson lifetime. The corresponding expression for model (b) is obtained by the replacement (d) \rightarrow (b) in (49).

The uncertainty of the branching fraction is estimated by independently varying the z -expansion parameters (the normalization and slope) of each form factor entering (49) over the ranges listed in Table 3, using three representative values for each parameter: central, maximal, and minimal. For every value of m_Ψ , the branching fraction is evaluated over the full parameter space, and the uncertainty is defined by the global minimum and maximum obtained in this sampling procedure. The resulting branching fractions for models (d) and (b) are shown in Fig. 4, where the uncertainty band is formed as explained above.

We compare our predictions with the ones in the LCSR- N approach [12]. For both results displayed in this figure, the effective Ψ -triquark couplings in the mesogenesis models (d) and (b) are set, for definiteness, to their maximum allowed values $|G_{(d)}|^2 = 1.0 \times 10^{-13}$ GeV⁻⁴, $|G_{(b)}|^2 = 4.7 \times 10^{-15}$ GeV⁻⁴. These values⁵ are equal to the upper limits, inferred, as explained in [2], from the ATLAS and CMS searches for heavy colored particles. The results of both LCSR approaches agree within large uncertainties. At the same time our predictions are systematically smaller and also have smaller uncertainties.

For numerical illustration, we quote the branching fractions obtained with our LCSR- B method at the benchmark value $m_\Psi = 2$ GeV and normalised to the corresponding

⁵Note that in [10, 12], equal couplings $|G_{(d)}|^2 = |G_{(b)}|^2 = 10^{-13}$ GeV⁻⁴ were used.

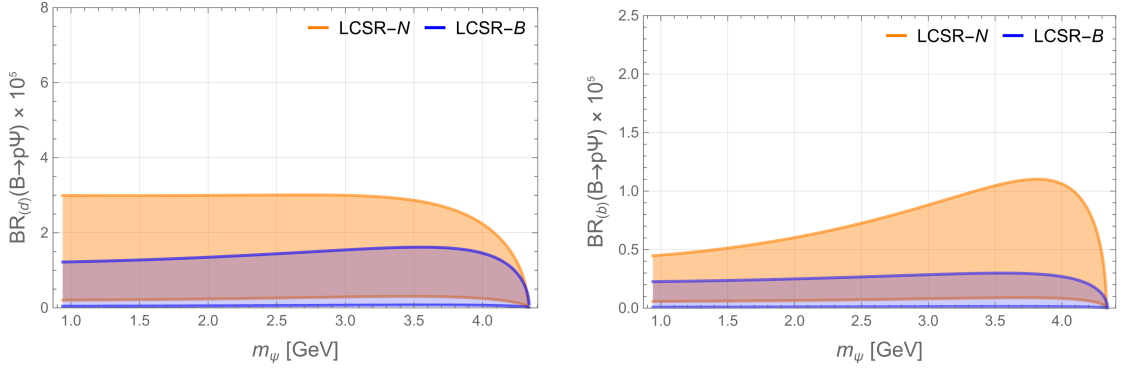


Figure 4: Branching fraction predicted for the $B^+ \rightarrow p\Psi$ decay in the model (d) (left panel) and model (b) (right panel). The blue bands represent the results of this work obtained with the LCSR-B method. For comparison, the orange bands show the results obtained using the method with nucleon DAs (LCSR-N).

coupling constants:

$$\begin{aligned} \text{BR}_{(d)}(B^+ \rightarrow p\Psi) &= \left(2.9_{-2.4}^{+10.0}\right) \left(\frac{|G_{(d)}|^2}{1.0 \times 10^{-13}}\right) \times 10^{-6}, \\ \text{BR}_{(b)}(B^+ \rightarrow p\Psi) &= \left(0.54_{-0.44}^{+2.0}\right) \left(\frac{|G_{(b)}|^2}{4.7 \times 10^{-15}}\right) \times 10^{-6}. \end{aligned} \quad (50)$$

6. Ratio of the $B^+ \rightarrow p\Psi$ width to inclusive width

Our predictions for the partial width of $B^+ \rightarrow p\Psi$ are not yet sufficient for a direct comparison with upper bounds measured for the $B^+ \rightarrow p + \text{invisible}$ decay. Indeed, the width is proportional to the square of the effective coupling $G_{(d)}$ or $G_{(b)}$, inherent to the model of mesogenesis (see (49)). For these couplings only the upper limits mentioned above are known. To enable a comparison with experiment independently of the coupling, it was suggested in [20] to consider the quantity

$$R_{[excl/incl]}(B^+ \rightarrow p\Psi) \equiv \frac{\text{BR}(B^+ \rightarrow p\Psi)}{\text{BR}(B^+ \rightarrow X_N\Psi)} \times 10^{-4}, \quad (51)$$

where the denominator contains the branching fraction of the inclusive decay $B \rightarrow X_N\Psi$. Here X_N denotes all possible and kinematically accessible hadronic states formed after the quark-level decay $\bar{b} \rightarrow ud\Psi$ by the diquark ud and by the spectator u -quark of B^+ -meson. The ratio of exclusive to inclusive widths in (51) is multiplied by a factor 10^{-4} , which is the minimal value of the inclusive branching fraction required for the realization of B -mesogenesis [2]. Evidently, in this ratio the effective couplings cancel each other. The idea put forward in [20] is to evaluate – at a given Ψ mass and within a

certain model of mesogenesis – the ratio of exclusive to inclusive widths, using available QCD-based methods for both widths. Then the quantity (51) directly yields a lower limit for the exclusive width:

$$\text{BR}(B^+ \rightarrow p\Psi) > R_{[excl/incl]}(B^+ \rightarrow p\Psi). \quad (52)$$

Comparing this limit with the measured upper bound, it is possible to determine the still allowed and/or already excluded values of the Ψ mass.

In [20], the inclusive rate $\text{BR}(B^+ \rightarrow X_N\Psi)$ was computed within the framework of the heavy quark expansion (HQE), where only the leading dimension-three term was included. The analysis was later improved in [21], by incorporating the power-suppressed contributions to the inclusive width up to dimension-six level. In both studies, the exclusive width entering the ratio was taken from [12], where LCSRs based on nucleon DAs were used.

Here, we revisit the estimate of $R_{[excl/incl]}$, using our updated exclusive widths obtained from LCSRs with B -meson DAs. Following [21], we include in the computation of the inclusive width the leading dimension-three term of HQE, as well as power-suppressed terms stemming from the dimension-five, dimension-six two-quark operators (the Darwin term), and also from the dimension-six four-quark operators. The detailed analysis of higher-dimensional terms in [21] reveals that the HQE remains reliable up to $m_\Psi \approx 2.0$ GeV for the model (d) and up to $m_\Psi \approx 3.0$ GeV for the model (b). Above these masses, subleading contributions to HQE become dominant and the whole expansion loses convergence.

Our results for models (d) and (b) are presented in Fig. 5, which shows the predicted lower limits for $\text{BR}(B^+ \rightarrow p\psi)$ as a function of the dark antibaryon mass m_Ψ , together with experimental upper bounds from BaBar [6] and Belle/Belle II [5]. Our new LCSR- B predictions for the exclusive branching fractions are smaller than the LCSR- N ones used in [20], leading to correspondingly smaller lower limits. In model (d), the lower limits can reach the level of $\sim 10^{-8}$, whereas model (b) yields limits of order 10^{-7} . As explained above, the intervals of Ψ mass above 2 GeV (3 GeV) for model (d) (model (b)) are not accessible to our estimate, due to inapplicability of the HQE method for the inclusive width.

The uncertainty of the predicted lower limit—represented by the band between the dashed and solid green lines in Fig. 5—is determined through the same procedure as employed for the exclusive branching fractions and described in Sec. 5.3. An additional 10% is assigned to account for residual theoretical uncertainty in the inclusive width calculation, including renormalization-scale dependence, scheme choices, and neglected higher-order perturbative and power corrections. Note that the overall uncertainty of the branching fraction is dominated by the form factors $F_{B \rightarrow pR}^{(d)}(0)$ and $F_{B \rightarrow pR}^{(b)}(0)$ computed in Sec. 5. Conservatively, we interpret the minimal value of the uncertainty band as our prediction for the lower limit of $\text{BR}(B^+ \rightarrow p\Psi)$.

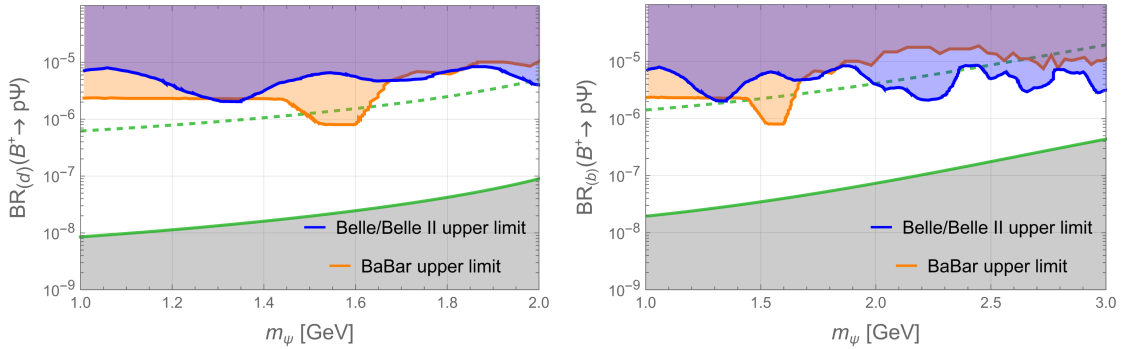


Figure 5: Branching fraction $\text{BR}(B^+ \rightarrow p\Psi)$ as a function of m_Ψ for model (d) (left panel) and model (b) (right panel). The solid green lines present the predicted lower limit (52), and the dashed green lines indicate maximal value of this limit within estimated uncertainties; orange and blue shaded regions display experimental upper limits set by, respectively, BaBar [6] and Belle/Belle II [5] measurements of the $B \rightarrow p + \text{invisible}$ decays. The white areas indicate the parameter space allowed by current experimental data.

7. Conclusion

In this paper, we applied the method of QCD light-cone sum rules (LCSRs) with B -meson distribution amplitudes (DAs) to the $B \rightarrow p$ transition form factors. These hadronic quantities are needed to evaluate the width of the exclusive $B^+ \rightarrow p\Psi$ decay predicted in the B -mesogenesis models. We considered two such models, (d) and (b), with different Ψ -triquark effective interactions.

LCSRs for these unusual baryon-to-meson form factors were obtained, expanding the underlying $B \rightarrow \text{vacuum}$ correlation function in terms of B -meson DAs, up to the twist-5 accuracy. We found that this correlation function has quite a peculiar operator-product expansion (OPE), as compared to traditional applications of this method to the $B \rightarrow \text{meson}$ form factors. First of all, the leading-order diagram contains a diquark loop, leading to logarithmic terms in the OPE. Moreover, the contributions of all three-particle (quark-antiquark-gluon) DAs up to twist-4 vanish. That is caused by several reasons: the form of the proton interpolating current, the scalar structure of the underlying effective operator, and the adopted limit of massless u, d quarks. We also found that the form factors in the two mesogenesis models are simply related by a factor of two. Altogether, the LCSRs for $B \rightarrow p$ form factors obey the hierarchy of twists, so that power corrections stemming from the subleading terms of light-cone expansion and expressed via twist-4,5 DAs are numerically suppressed, albeit moderately, with respect to the leading contributions from the twist-2,3 DAs.

For the hadronic part of our sum rules, describing the channel of the proton interpolating current, we adopted the same ansatz as in the LCSRs for the nucleon electromagnetic form factors, in which all excited nucleon states are included in the continuum and ap-

proximated by quark-hadron duality.

For the two $B \rightarrow p$ form factors relevant for the $B \rightarrow p\Psi$ decay width, we produced numerical results in the region of the LCSR validity at negative momentum transfer squared. The form factors in the physical region of that decay were then evaluated by fitting the LCSR results to a standard z -expansion and by the subsequent extrapolation of the latter.

Our results for $B \rightarrow p$ form factors are compared with the ones from the alternative method of LCSRs with nucleon DAs (LCSR- N). The latter sum rules, especially the ones for the model (b), reveal an anomalously large higher-twist contributions with still uncertain parameters, making the LCSR- N method somewhat less reliable than the LCSR- B method applied in this paper. Nevertheless, the widths predicted from the two approaches and for both models (d) and (b) agree within large uncertainties. Numerically, the range of $B^+ \rightarrow p\Psi$ branching fractions obtained in this work is smaller and narrower.

Apart from predictions for the exclusive $B^+ \rightarrow p\Psi$ decay width as a function of the Ψ mass and effective coupling, we evaluated the important ratio of exclusive to inclusive branching fractions, employing the available heavy quark expansion (HQE) result for inclusive widths. This ratio yields lower bounds for the $B^+ \rightarrow p\Psi$ branching fraction, independent of the value of the effective Ψ -triquark coupling. Comparison with existing experimental upper bounds reveals that there is still a large gap between upper and lower bounds in the region of small Ψ masses.

Further improvements and extensions of LCSRs obtained in this paper are possible. In particular, more accurate estimates of the two key parameters: the inverse moment of the B -meson twist-2 DA and the nucleon decay constant, will decrease the parametric uncertainty of LCSRs. Furthermore, a more detailed resonance pattern of the hadronic spectral density in the sum rule will open up a possibility to estimate also the form factors of the $B \rightarrow N^*(1535)$ and $B \rightarrow N(1440)$ transitions.

Most importantly, the LCSRs with B -meson DAs can be straightforwardly extended to evaluate the form factors of $B \rightarrow \Lambda$ or $B \rightarrow \Lambda_c$ transitions, using the interpolating three-quark current with a suitable quark-flavour combination. This framework can therefore be applied to the $B \rightarrow \Lambda\Psi$ and $B^+ \rightarrow \Lambda_c^+\Psi$ decay modes predicted in various flavour realizations of B -mesogenesis models.⁶

In the absence of lattice QCD calculations of $B \rightarrow p$ form factors, LCSRs remain the only QCD-based method to provide hadronic input to the studies of $B^+ \rightarrow p\Psi$ and similar invisible B -meson decays. Our results obtained from these sum rules indicate that future progress in two directions – reducing the uncertainty of the theoretical lower limits and decreasing the experimental upper limits by at least an order of magnitude – could provide a decisive test of the B -mesogenesis scenario.

⁶In this context it is worth mentioning the recent application [35] of LCSRs with the Λ_b DAs, introduced in [36], to the form factors of $\Lambda_b \rightarrow \pi, K$ transitions, relevant for the $\Lambda_b \rightarrow \pi\Psi$ and $\Lambda \rightarrow K\Psi$ decays.

Acknowledgments

We thank Alexander Lenz for useful and stimulating discussions. This work was supported by the Deutsche Forschungsgemeinschaft (DFG, German Research Foundation) under the grant 396021762 - TRR 257.

A. B -meson distribution amplitudes

A.1. Two-particle DAs

We use the following decomposition [13] of the B^+ -to-vacuum matrix element in HQET:

$$\begin{aligned} \langle 0 | \bar{h}_{v\alpha}(0) [0, x] u_\beta(x) | B^+(v) \rangle &= \frac{if_B m_B}{4} \int_0^\infty d\omega e^{-i\omega v \cdot x} \left[\left\{ \phi_+^B(\omega) + x^2 g_+^B(\omega) \right\} [(1 + \not{v}) \gamma_5]_{\beta\alpha} \right. \\ &\quad \left. - \frac{1}{2v \cdot x} \left\{ \phi_+^B(\omega) - \phi_-^B(\omega) + x^2 (g_+^B(\omega) - g_-^B(\omega)) \right\} [\not{x}(1 + \not{v}) \gamma_5]_{\beta\alpha} \right]. \end{aligned} \quad (\text{A.1})$$

In the above, $[0, x]$ is the gauge link, and the variable ω is the light-cone projection of the light-quark momentum in the heavy-meson rest frame.

The functions $\phi_+^B(\omega)$, $\phi_-^B(\omega)$, $g_+^B(\omega)$ and $g_-^B(\omega)$ are, respectively, the DAs of twist two, three, four and five, according to the nomenclature of [14]. The normalization conditions for the first two DAs are:

$$\int_0^\infty d\omega \phi_\pm^B(\omega) = 1. \quad (\text{A.2})$$

The decomposition (A.1) is rearranged into an equivalent form without the factors $1/(v \cdot x)$, by introducing the integrated linear combination of the twist-2 and twist-3 DAs [16]:

$$\Phi_\pm^B(w) \equiv \int_0^w d\tau \left(\phi_+^B(\tau) - \phi_-^B(\tau) \right), \quad (\text{A.3})$$

so that

$$\frac{d\Phi_\pm^B(w)}{dw} = \phi_+^B(w) - \phi_-^B(w), \quad \Phi_\pm^B(0) = \Phi_\pm^B(\infty) = 0. \quad (\text{A.4})$$

We also use analogous definition for the combination of twist-four and twist-five DAs:

$$G_\pm^B(w) \equiv \int_0^w d\tau \left(g_+^B(\tau) - g_-^B(\tau) \right). \quad (\text{A.5})$$

Note that performing charge conjugation of the matrix element in (A.1), we restore for the twist-two and twist-three parts the definition of B^- -meson DAs used e.g. in [37, 16].

In this paper we use the standard exponential model [13] of the twist-two DA:

$$\phi_+^B(\omega) = \frac{\omega}{\lambda_B^2} e^{-\omega/\lambda_B}. \quad (\text{A.6})$$

For the twist-three and twist-four DAs we employ the corresponding exponential form suggested in [14]:

$$\phi_-^B(\omega) = \frac{1}{\lambda_B} e^{-\omega/\lambda_B} + \frac{1}{2\lambda_B} \left[1 - \frac{2\omega}{\lambda_B} + \frac{\omega^2}{2\lambda_B^2} \right] \frac{1-R}{1+2R} e^{-\omega/\lambda_B}, \quad (\text{A.7})$$

$$g_+^B(\omega) = \frac{3\omega^2}{16\lambda_B} \frac{3+4R}{1+2R} e^{-\omega/\lambda_B}. \quad (\text{A.8})$$

Finally, for the twist-five DA we adopt the same exponential form based on Wandzura-Wilczek approximation, as in [17]:

$$g_-^B(\omega) = \frac{3\omega}{4} e^{-\omega/\lambda_B}. \quad (\text{A.9})$$

To assess the role of twist-five contribution in the numerical analysis, we also omit the term with g_-^B in the correlation function. This step is reduced to a simple replacement:

$$G_{\pm}^B(\omega) \rightarrow G_+^B(\omega) = \int_0^{\omega} d\tau g_+^B(\tau) \quad (\text{A.10})$$

in (33) and (34).

The set of B -meson DAs used here is determined by three parameters. The first one is the B -meson decay constant, very accurately computed in lattice QCD; the second one is the inverse moment of the twist-2 DA:

$$\frac{1}{\lambda_B} = \int_0^{\infty} d\omega \frac{\phi_+^B(\omega)}{\omega}. \quad (\text{A.11})$$

The adopted value quoted in Table 1 was obtained [30] at the scale ~ 1 GeV, and here we neglect the scale dependence for simplicity, having in mind the currently large uncertainty of the available determination. The third parameter is the ratio

$$R \equiv \lambda_E^2 / \lambda_H^2, \quad (\text{A.12})$$

where $\lambda_{E,H}$ parameterize the vacuum-to- B matrix elements of the heavy-light quark-antiquark-gluon operators. Their definitions and the first estimates can be found in [13]. These estimates were obtained, employing QCD sum rules in HQET for a nondiagonal correlation function, in which the product of a quark-antiquark-gluon operator is correlated with the B -meson interpolating quark-antiquark current. These determinations were improved in two different directions: in [32], adding NLO corrections to the nondiagonal sum rules and in [33], employing diagonal correlation functions. The results only

marginally agree, therefore we take an average of both. As inputs for averaging we take the three intervals given by $\lambda_E^2(1 \text{ GeV}) = 0.03 \pm 0.02 \text{ GeV}^2$, $\lambda_H^2(1 \text{ GeV}) = 0.06 \pm 0.03 \text{ GeV}^2$ from [32] and $R = 0.1 \pm 0.1$ from [33]. Assuming all these intervals are uniformly distributed and uncorrelated, we used a large (10^5) sample of points from the first two of them, and obtain a distribution for R calculated from (A.12). A similar sample for this parameter was also drawn directly from the third interval. The resulting range for R quoted in Table 1 was inferred from the distribution of the arithmetic mean of these samples, with the central value corresponding to the median and the uncertainties corresponding to the 68.27% (1σ) deviation. Our estimate is consistent with previous one $R = 0.4_{-0.3}^{+0.5}$ from [38] determined differently, using as inputs the sum rule results from [13] and [32].

A.2. Three-particle DAs

We use the $B \rightarrow \text{vacuum}$ matrix element expanded in terms of three-particle (quark-antiquark-gluon) DAs with twist-4 accuracy that was originally obtained in [14]. More specifically, we use the expression of this expansion for \bar{B} meson from [38], rewriting it with free Dirac indices and charge-conjugating to the matrix element with B^+ meson:

$$\begin{aligned}
\langle 0 | \bar{h}_{\nu\alpha}(0) g_s \frac{\lambda^a}{2} G_{\mu\nu}^a(u x) q_\beta(x) | B^+(v) \rangle &= -\frac{f_B m_B}{4} \int_0^\infty d\omega_1 \int_0^\infty d\omega_2 e^{-i(\omega_1 + u\omega_2)v \cdot x} \\
&\times \left\{ \gamma_5 \left[-(v_\mu \gamma_\nu - v_\nu \gamma_\mu) \phi_3 - \frac{i}{2} \sigma_{\mu\nu} [\phi_3 - \phi_4] + \frac{x_\mu v_\nu - x_\nu v_\mu}{2v \cdot x} [\phi_3 + \phi_4 - 2\psi_4] \right. \right. \\
&+ \frac{x_\mu \gamma_\nu - x_\nu \gamma_\mu}{2v \cdot x} [\phi_3 + \tilde{\psi}_4] + \frac{i\epsilon_{\mu\nu\alpha\beta} x^\alpha v^\beta}{2v \cdot x} \gamma_5 [\phi_3 - \phi_4 + 2\tilde{\psi}_4] \\
&- \frac{i\epsilon_{\mu\nu\alpha\beta} x^\alpha}{2v \cdot x} \gamma^\beta \gamma_5 [\phi_3 - \phi_4 + \tilde{\psi}_4] + \frac{(x_\mu v_\nu - x_\nu v_\mu) \not{x}}{2(v \cdot x)^2} [\phi_4 - \psi_4 - \tilde{\psi}_4] \\
&\left. \left. - \frac{\not{x}(x_\mu \gamma_\nu - x_\nu \gamma_\mu)}{4(v \cdot x)^2} [\phi_3 - \phi_4 + 2\tilde{\psi}_4] \right] (1 - \not{v}) \right\}_{\beta\alpha}. \tag{A.13}
\end{aligned}$$

In the above, ϕ_3 is the DA of twist-3, and the three DAs of twist-4 are ϕ_4 , ψ_4 and $\tilde{\psi}_4$. For brevity, their dependence on ω_1, ω_2 is not shown, as well as the Wilson lines on left-hand side.

In analogy to (A.3) and (A.5), we define the integrated DAs,

$$\bar{\Phi}(\omega_1, \omega_2) = \int_0^{\omega_1} d\tau \Phi(\tau, \omega_2), \tag{A.14}$$

where $\Phi = \{\phi_3, \phi_4, \psi_4, \tilde{\psi}_4\}$. This time we repeat this procedure twice to get rid of the second power of $(1/v \cdot x)$ in (A.13), introducing DAs with double bars:

$$\bar{\bar{\Phi}}(\omega_1, \omega_2) = \int_0^{\omega_1} d\tau \bar{\Phi}(\tau, \omega_2). \tag{A.15}$$

Applying (A.14) and (A.15), it is possible, – as it was done in [38] – to transform the equation (A.13) to a more convenient form, free of $(v \cdot x)$ in denominators:

$$\begin{aligned}
\langle 0 | \bar{h}_{v\alpha}(0) g_s \frac{\lambda^a}{2} G_{\mu\nu}^a(ux) q_\beta(x) | B^+(v) \rangle &= -\frac{f_B m_B}{4} \int_0^\infty d\omega_1 d\omega_2 e^{-i\sigma m_B v \cdot x} \\
&\times \left\{ \gamma_5 \left[-(v_\mu \gamma_\nu - v_\nu \gamma_\mu) \phi_3 - \frac{i}{2} \sigma_{\mu\nu} [\phi_3 - \phi_4] + \frac{i}{2} (x_\mu v_\nu - x_\nu v_\mu) [\bar{\phi}_3 + \bar{\phi}_4 - 2\bar{\psi}_4] \right. \right. \\
&+ \frac{i}{2} (x_\mu \gamma_\nu - x_\nu \gamma_\mu) [\bar{\phi}_3 + \bar{\psi}_4] - \frac{1}{2} \epsilon_{\mu\nu\alpha\beta} x^\alpha v^\beta \gamma_5 [\bar{\phi}_3 - \bar{\phi}_4 + 2\bar{\psi}_4] \\
&+ \frac{1}{2} \epsilon_{\mu\nu\alpha\beta} x^\alpha \gamma^\beta \gamma_5 [\bar{\phi}_3 - \bar{\phi}_4 + \bar{\psi}_4] - \frac{1}{2} (x_\mu v_\nu - x_\nu v_\mu) \not{x} [\bar{\phi}_4 - \bar{\psi}_4 - \bar{\bar{\psi}}_4] \\
&\left. \left. + \frac{1}{4} \not{x} (x_\mu \gamma_\nu - x_\nu \gamma_\mu) [\bar{\phi}_3 - \bar{\phi}_4 + 2\bar{\bar{\psi}}_4] \right] (1 - \not{\psi}) \right\}_{\beta\alpha}, \tag{A.16}
\end{aligned}$$

where we introduce the new variable

$$\sigma(u, \omega_1, \omega_2) \equiv (\omega_1 + u \omega_2) / m_B. \tag{A.17}$$

The exponential model (A.6) was extended to the three-particle B -meson DAs in [14], and we present that model here for completeness, although we will not use them due to vanishing of three-particle DAs contributions to our correlation function (see Sec. 4.2). We have:

$$\begin{aligned}
\phi_3(\omega_1, \omega_2) &= -\frac{3\omega_1\omega_2^2}{4\lambda_B^3} \frac{1-R}{1+2R} e^{-(\omega_1+\omega_2)/\lambda_B} \\
\phi_4(\omega_1, \omega_2) &= \frac{3\omega_2^2}{4\lambda_B^2} \frac{1+R}{1+2R} e^{-(\omega_1+\omega_2)/\lambda_B} \\
\psi_4(\omega_1, \omega_2) &= R \tilde{\psi}_4(\omega_1, \omega_2) = \frac{3\omega_1\omega_2}{2\lambda_B^2} \frac{R}{1+2R} e^{-(\omega_1+\omega_2)/\lambda_B}. \tag{A.18}
\end{aligned}$$

Note that all three-particle DAs in this model are characterized by two input parameters, λ_B and R , the same as in the two-particle DAs.

Finally, we present the coefficients in the expression (36) for one of the diagrams with three-particle DAs:

$$\begin{aligned}
\mathcal{C}(\mathcal{P}, v) &= [8(\mathcal{P} \cdot v) \not{\mathcal{P}} \not{\psi} - 16(\mathcal{P} \cdot v)^2] \phi_3 + 8(\mathcal{P} \cdot v - \not{\mathcal{P}} \not{\psi}) (\bar{\phi}_3 - \bar{\phi}_4) + 8(4\mathcal{P} \cdot v - \not{\mathcal{P}} \not{\psi}) \bar{\psi}_4 \\
&\quad - \frac{4}{\mathcal{P}^2} [\mathcal{P}^2 + 2(\mathcal{P} \cdot v) \not{\mathcal{P}} \not{\psi}] (\bar{\phi}_4 - \bar{\bar{\psi}}_4 - \bar{\bar{\psi}}_4) - 12(\bar{\phi}_3 - \bar{\phi}_4 + 2\bar{\bar{\psi}}_4), \\
\bar{\mathcal{C}}(\mathcal{P}, v) &= 12\mathcal{P}^2 \text{Log}(-\mathcal{P}^2) \phi_4 - 4(\mathcal{P} \cdot v - \not{\mathcal{P}} \not{\psi}) (\bar{\phi}_3 - \bar{\phi}_4) - 4(4\mathcal{P} \cdot v - \not{\mathcal{P}} \not{\psi}) \bar{\psi}_4 \\
&\quad + \frac{4}{\mathcal{P}^2} [\mathcal{P}^2 + 2(\mathcal{P} \cdot v) \not{\mathcal{P}} \not{\psi}] (\bar{\phi}_4 - \bar{\psi}_4 - \bar{\bar{\psi}}_4) + 12(\bar{\phi}_3 - \bar{\phi}_4 + 2\bar{\bar{\psi}}_4), \tag{A.19}
\end{aligned}$$

where $\mathcal{P} \equiv P - \sigma m_B v$. In these expressions, terms without an imaginary part in \mathcal{P}^2 are omitted since they do not contribute to the LCSRs. Note however, that the relations (37) and (38) for three-particle contributions are valid including these terms.

B. Transformation to a form of dispersion integral

To transform the amplitudes (31) and (32) into a dispersion form, we subdivide their expressions into similar terms with respect to analytic properties in the variable P^2 .

For the terms that contain $s(\omega) - P^2$ in denominator the transformation is most easily done. For each term of this type multiplied by a certain function $g(\omega)$ we use the transformation $\omega \rightarrow s(\omega)$ and obtain:

$$\int_0^\infty d\omega \frac{g(\omega)}{s(\omega) - P^2} = \int_0^\infty \frac{ds}{s - P^2} \frac{d\omega(s)}{ds} g(\omega(s)). \quad (\text{B.1})$$

To obtain a dispersion form for the terms in (31) and (32) with a logarithmic dependence on P^2 , it is sufficient to consider the integral:

$$I_{(f)}(P^2) \equiv \int_0^\infty d\omega \ln[s(\omega) - P^2] f(\omega) = \int_0^\infty ds \ln[s - P^2] \frac{d\omega(s)}{ds} f(\omega(s)), \quad (\text{B.2})$$

where $f(\omega)$ is a function containing one of the DAs. Employing

$$\frac{1}{\pi} \text{Im}_{P^2}(\ln[s - P^2]) = -\theta(P^2 - s),$$

and returning in (B.2) to the initial integration variable ω , we obtain:

$$\frac{1}{\pi} \text{Im} I_{(f)}(s) = - \int_0^{\omega(s)} d\omega' f(\omega'), \quad (\text{B.3})$$

yielding the dispersion form of that integral:

$$I_{(f)}(P^2) = - \int_0^\infty \frac{ds}{s - P^2} \int_0^{\omega(s)} d\omega' f(\omega'), \quad (\text{B.4})$$

Note that the integral over s is divergent on the upper limit, but that is not relevant for our purposes, because this divergence will be eliminated by the Borel transform $P^2 \rightarrow M^2$. In other words, the dispersion integral needs subtractions, and since subtraction terms are dependent on polynomials in P^2 , they vanish after that transform. For the same reason, the terms in (31), containing an extra factor P^2 multiplying the above integral are easily transformed to the dispersion form by replacing $P^2 \rightarrow s$, and

$$P^2 I_{(f)}(P^2) \rightarrow - \int_0^\infty ds \frac{s}{s - P^2} \int_0^{\omega(s)} d\omega' f(\omega'). \quad (\text{B.5})$$

Still it is important to convince ourselves that after Borel transform both expressions, (B.4) and (B.2) are equal. For this purpose, we derive the Borel transform for the logarithmic function entering (B.2):

$$\mathcal{B}_{M^2} \left(\ln [s(\omega) - P^2] \right) = \int_0^{s(\omega)} ds' e^{-s'/M^2} - M^2. \quad (\text{B.6})$$

This formula is obtained if one uses (B.4) and the analogous expression for the imaginary part of $\ln[-P^2]$ and then takes the difference of two dispersion relations, yielding:

$$\ln [s(\omega) - P^2] - \ln [-P^2] = \int_0^{s(\omega)} \frac{ds'}{s' - P^2}. \quad (\text{B.7})$$

The Borel transform of this equation, together with the well familiar formula

$$\mathcal{B}_{M^2} \ln [-P^2] = -M^2,$$

yields then (B.6). Applying the latter formula to the integral (B.2), we obtain

$$\mathcal{B}_{M^2}(I_{(f)}(P^2)) = -M^2 \int_0^\infty d\omega e^{-s(\omega)/M^2} f(\omega). \quad (\text{B.8})$$

It remains to apply the same Borel transform to the dispersion form (B.4):

$$\mathcal{B}_{M^2}(I_{(f)}(P^2))_{disp} = - \int_0^\infty ds e^{-s/M^2} \int_0^{\omega(s)} d\omega' f(\omega'). \quad (\text{B.9})$$

As a final step of our proof, this equality is reduced to (B.8) by a simple permutation of the integration variables s and ω' .

References

- [1] G. Elor, M. Escudero, and A. Nelson, *Baryogenesis and Dark Matter from B Mesons*, *Phys. Rev. D* **99** (2019), no. 3 035031, [arXiv:1810.00880].
- [2] G. Alonso-Álvarez, G. Elor, and M. Escudero, *Collider signals of baryogenesis and dark matter from B mesons: A roadmap to discovery*, *Phys. Rev. D* **104** (2021), no. 3 035028, [arXiv:2101.02706].
- [3] F. Elahi, G. Elor, and R. McGehee, *Charged B mesogenesis*, *Phys. Rev. D* **105** (2022), no. 5 055024, [arXiv:2109.09751].
- [4] G. Alonso-Álvarez, G. Elor, M. Escudero, B. Fornal, B. Grinstein, and J. Martin Camalich, *Strange physics of dark baryons*, *Phys. Rev. D* **105** (2022), no. 11 115005, [arXiv:2111.12712].
- [5] **Belle-II**, **Belle** Collaboration, M. Abumusabh et al., *A search for feebly-interacting particles in B decays with missing energy at Belle*, arXiv:2601.07104.
- [6] **BaBar** Collaboration, J. P. Lees et al., *Search for Evidence of Baryogenesis and Dark Matter in $B^+ \rightarrow \psi_D + p$ Decays at BABAR*, *Phys. Rev. Lett.* **131** (2023), no. 20 201801, [arXiv:2306.08490].
- [7] **BaBar** Collaboration, J. P. Lees et al., *Search for B mesogenesis at BaBar*, *Phys. Rev. D* **107** (2023), no. 9 092001, [arXiv:2302.00208].
- [8] **BaBar** Collaboration, J. P. Lees et al., *Search for baryogenesis and dark matter in $B^+ \rightarrow \Lambda c^+ + \text{invisible}$ decays*, *Phys. Rev. D* **111** (2025), no. 3 L031101, [arXiv:2412.06950].
- [9] **Belle** Collaboration, C. Hadjivasiliou et al., *Search for B^0 meson decays into Λ and missing energy with a hadronic tagging method at Belle*, *Phys. Rev. D* **105** (2022), no. 5 L051101, [arXiv:2110.14086].
- [10] A. Khodjamirian and M. Wald, *B-meson decay into a proton and dark antibaryon from QCD light-cone sum rules*, *Phys. Lett. B* **834** (2022) 137434, [arXiv:2206.11601].
- [11] G. Elor and A. W. M. Guerrero, *Branching fractions of B meson decays in Mesogenesis*, *JHEP* **02** (2023) 100, [arXiv:2211.10553].
- [12] A. Boushmelev and M. Wald, *Higher twist corrections to B-meson decays into a proton and dark antibaryon from QCD light-cone sum rules*, *Phys. Rev. D* **109** (2024), no. 5 055049, [arXiv:2311.13482].
- [13] A. G. Grozin and M. Neubert, *Asymptotics of heavy meson form-factors*, *Phys. Rev. D* **55** (1997) 272–290, [hep-ph/9607366].

- [14] V. M. Braun, Y. Ji, and A. N. Manashov, *Higher-twist B-meson Distribution Amplitudes in HQET*, *JHEP* **05** (2017) 022, [arXiv:1703.02446].
- [15] A. Khodjamirian, T. Mannel, and N. Offen, *B-meson distribution amplitude from the $B \rightarrow \pi$ form-factor*, *Phys. Lett. B* **620** (2005) 52–60, [hep-ph/0504091].
- [16] A. Khodjamirian, T. Mannel, and N. Offen, *Form-factors from light-cone sum rules with B-meson distribution amplitudes*, *Phys. Rev. D* **75** (2007) 054013, [hep-ph/0611193].
- [17] N. Gubernari, A. Kokulu, and D. van Dyk, *$B \rightarrow P$ and $B \rightarrow V$ Form Factors from B-Meson Light-Cone Sum Rules beyond Leading Twist*, *JHEP* **01** (2019) 150, [arXiv:1811.00983].
- [18] S. Faller, A. Khodjamirian, C. Klein, and T. Mannel, *$B \rightarrow D^{(*)}$ Form Factors from QCD Light-Cone Sum Rules*, *Eur. Phys. J. C* **60** (2009) 603–615, [arXiv:0809.0222].
- [19] A. Khodjamirian, B. Melić, and Y.-M. Wang, *A guide to the QCD light-cone sum rules for b-quark decays*, *Eur. Phys. J. ST* **233** (2024), no. 2 271–298, [arXiv:2311.08700].
- [20] A. Lenz, A. Mohamed, and Z. Wüthrich, *Constraining B-mesogenesis models with inclusive and exclusive decays*, *JHEP* **08** (2025) 141, [arXiv:2412.14947].
- [21] A. Mohamed, *Are Subleading Effects Really Subleading? B-Meson Decays in Mesogenesis*, arXiv:2511.04858.
- [22] B. L. Ioffe, *Calculation of Baryon Masses in Quantum Chromodynamics*, *Nucl. Phys. B* **188** (1981) 317–341. [Erratum: *Nucl.Phys.B* 191, 591–592 (1981)].
- [23] **Particle Data Group** Collaboration, S. Navas et al., *Review of particle physics*, *Phys. Rev. D* **110** (2024), no. 3 030001.
- [24] I. V. Anikin, V. M. Braun, and N. Offen, *Nucleon Form Factors and Distribution Amplitudes in QCD*, *Phys. Rev. D* **88** (2013) 114021, [arXiv:1310.1375].
- [25] V. M. Braun, A. Lenz, N. Mahnke, and E. Stein, *Light cone sum rules for the nucleon form-factors*, *Phys. Rev. D* **65** (2002) 074011, [hep-ph/0112085].
- [26] I. I. Balitsky and V. M. Braun, *Evolution Equations for QCD String Operators*, *Nucl. Phys. B* **311** (1989) 541–584.
- [27] D. Espriu, P. Pascual, and R. Tarrach, *Baryon Masses and Chiral Symmetry Breaking*, *Nucl. Phys. B* **214** (1983) 285–298.
- [28] A. Lenz, M. Gockeler, T. Kaltenbrunner, and N. Warkentin, *The Nucleon Distribution Amplitudes and their application to nucleon form factors and the $N \rightarrow \Delta$ transition at intermediate values of Q^2* , *Phys. Rev. D* **79** (2009) 093007, [arXiv:0903.1723].

- [29] **Flavour Lattice Averaging Group (FLAG)** Collaboration, Y. Aoki et al., *FLAG Review 2024*, [arXiv:2411.04268](#).
- [30] V. M. Braun, D. Y. Ivanov, and G. P. Korchemsky, *The B meson distribution amplitude in QCD*, *Phys. Rev. D* **69** (2004) 034014, [[hep-ph/0309330](#)].
- [31] A. Khodjamirian, R. Mandal, and T. Mannel, *Inverse moment of the B_s -meson distribution amplitude from QCD sum rule*, *JHEP* **10** (2020) 043, [[arXiv:2008.03935](#)].
- [32] T. Nishikawa and K. Tanaka, *QCD Sum Rules for Quark-Gluon Three-Body Components in the B Meson*, *Nucl. Phys. B* **879** (2014) 110–142, [[arXiv:1109.6786](#)].
- [33] M. Rahimi and M. Wald, *QCD sum rules for parameters of the B-meson distribution amplitudes*, *Phys. Rev. D* **104** (2021), no. 1 016027, [[arXiv:2012.12165](#)].
- [34] C. Bourrely, I. Caprini, and L. Lellouch, *Model-independent description of $B \rightarrow \pi \ell \nu$ decays and a determination of $|V(ub)|$* , *Phys. Rev. D* **79** (2009) 013008, [[arXiv:0807.2722](#)]. [Erratum: *Phys.Rev.D* 82, 099902 (2010)].
- [35] Y.-J. Shi, Y. Xing, and Z.-P. Xing, *Heavy baryon decays into light meson and dark baryon within LCSR*, *Eur. Phys. J. C* **84** (2024), no. 3 306, [[arXiv:2401.14120](#)].
- [36] P. Ball, V. M. Braun, and E. Gardi, *Distribution Amplitudes of the Lambda(b) Baryon in QCD*, *Phys. Lett. B* **665** (2008) 197–204, [[arXiv:0804.2424](#)].
- [37] M. Beneke and T. Feldmann, *Symmetry breaking corrections to heavy to light B meson form-factors at large recoil*, *Nucl. Phys. B* **592** (2001) 3–34, [[hep-ph/0008255](#)].
- [38] S. Descotes-Genon, A. Khodjamirian, and J. Virto, *Light-cone sum rules for $B \rightarrow K\pi$ form factors and applications to rare decays*, *JHEP* **12** (2019) 083, [[arXiv:1908.02267](#)].